T.R.
GEBZE TECHNICAL UNIVERSITY
GRADUATE SCHOOL OF NATURAL AND APPLIED SCIENCES

DESIGN OPTIMIZATION OF A PLASTIC COVER UNDER IMPACT LOADING

UĞUR ŞAHİNKAYA

A THESIS SUBMITTED FOR THE DEGREE OF
MASTER OF SCIENCE
DEPARTMENT OF MECHANICAL ENGINEERING

GEBZE
2022

T.R.

GEBZE TECHNICAL UNIVERSITY

GRADUATE SCHOOL OF NATURAL AND APPLIED SCIENCES

DESIGN OPTIMIZATION OF A PLASTIC COVER UNDER IMPACT LOADING

UĞUR ŞAHİNKAYA

A THESIS SUBMITTED FOR THE DEGREE OF MASTER OF SCIENCE

DEPARTMENT OF MECHANICAL ENGINEERING

THESIS SUPERVISOR

ASSOC. PROF. DR. AHMET SİNAN ÖKTEM

GEBZE

2022

T.C.

GEBZE TEKNİK ÜNİVERSİTESİ

FEN BİLİMLERİ ENSTİTÜSÜ

DARBE YÜKÜ ALTINDAKİ PLASTİK BİR KAPAĞIN TASARIM OPTİMİZASYONU

UĞUR ŞAHİNKAYA

YÜKSEK LİSANS TEZİ

MAKİNE MÜHENDİSLİĞİ ANABİLİM DALI

DANIŞMANI

DOÇ. DR. AHMET SİNAN ÖKTEM

GEBZE

2022

GEBZE TEKNİK ÜNİVERSİTESİ	**YÜKSEK LİSANS JÜRİ ONAY FORMU**

GTÜ Fen Bilimleri Enstitüsü Yönetim Kurulu'nun 10/02/2022 tarih ve . 2022/10 sayılı kararıyla oluşturulan jüri tarafından 27/05/2022 tarihinde tez savunma sınavı yapılan Uğur ŞAHİNKAYA'nın tez çalışması Makina Mühendisliği Anabilim Dalında YÜKSEK LİSANS tezi olarak kabul edilmiştir.

JÜRİ

ÜYE
(TEZ DANIŞMANI) : Doç.Dr. Ahmet Sinan ÖKTEM

ÜYE : Dr. Öğr. Üyesi Recep ÖNLER

ÜYE : Prof. Dr. Hasan KURTARAN

ONAY

Gebze Teknik Üniversitesi Fen Bilimleri Enstitüsü Yönetim Kurulu'nun

...…/….../……… tarih ve ……./…..... sayılı kararı.

İMZA/MÜHÜR

SUMMARY

Vehicle rear axle is usually under impact loading during drive due to stone chipping. Stone chipping causes wearing and corrosion on rear axle environment. Rear axle compartment is usually protected with plastic covers.

Rear axle covers are usually produced with recycled polypropylene (PP), which have low mechanical characteristics. Breakage of PP rear axle covers under impact loading are often encountered. Dynamic performance tests of rear axle covers are performed with physical vehicle road tests and there is no existing procedure to control whether the cover is design to meet performance criteria or not. The fact that the tests are carried out after the production of the injection mould leads to time and cost losses, considering the different road and material conditions.

In this thesis, mechanical behaviour of plastic cover under impact loading is examined experimentally with different impactor types and with finite element analysis in computer environment. In the scope of this study, response surface of Von Misses stress is plotted from geometrical parameters. It is aimed to design a lightweight, optimum rear axle cover that can meet the mechanical strength requirements. Weight is directly related to the thickness parameter. The second parameter that determines the product geometry is the relative angular orientation of the impactor and target plate. It is determined by the angle parameter. The part was modelled parametrically and the thickness and angle values providing the optimum design were investigated.

Key Words: Dynamic loading, Polypropylene, Stone chipping, Structural Optimization, Curve Fitting, Finite Element Analysis.

ÖZET

Otomobil arka aksının taş yükünü maruz kalması sık rastlanan bir durumdur. Taş yükü araç arka aksamında aşınma ve korozoyona sebep olmaktadır. Araç arka aksı genellikle koruyucu plastik kapaklarla korunmaktadır.

Otomobil arka aksını koruyan plastik kapaklar genellelikle düşük mekanik davranışına sahip geri dönüşüm plastiğinden üretilmiş polipropilen (PP) malzelerden üretilmektedirler. Bu PP koruyucu kapakların darbe yükü ile kırılması sıkça rastlanan bir durumdur. Plastik koruyucu kapakların darbe yüküne dayanımı fiziksel araç testleri ile kontrol edilmektedir ve hali hazırda performans kriterlerine uygun tasarım yapılıp yapılmadığı kontrol edilemememektedir. Fiziki testlerin kalıp imalatından sonra gerçekleşiyor olması ve çeşitli malzeme, yol durumu senaryosunun dikkate alınarak testlerin gerçekleştirilmesi maliyet ve zaman kayıplarına yol açmaktadır.

Bu tez darbe yüküne maruz kalan plastik bir koruyucu kapağın farklı çarpan parçalar dikkate alınarak mekanik dayanımlarının incelenmesi ve sonlu elemanlar yöntemi ile analizi ile ilgilidir. Çalışma kapsamında sonlu elemanlar yöntemiyle elde edilen sonuçlarla eğri uydurularak plastik koruyucu kapağın en iyi tasarımının yapılması hedeflenmiştir.

Plastik koruyucu kapağın en iyi tasarımı ağırlık sınırlandırılarak yapılmıştır. Ağırlık, kalınlık değişkeni ile tayin edilmiştir. Parça geometrisi ise parametrik olarak tasarlanmıştır ve en iyi tasarım parça geometrisini etkileyen parametrelerin ve kalınlığın en iyilenmesi ile belirlenmiştir.

Anahtar Kelimeler: Polipropilen, Taş Yükü, Kırılma, Sonlu Elemanlar Analizi, Yapısal Optimizasyon, Eğri Uydurma.

ACKNOWLEDGEMENTS

I appreciated the support of assoc. prof. Ahmet Sinan ÖKTEM. I thank him for his understanding and encouragement to finish my tasks on time in correct way all the time. I am also thankful to Prof. Dr. Hasan KURTARAN for teaching me finite element analysis and numerical analysis and for being committee member. I would like to thank the committee member Dr. Recep Önler for his valuable feedback and contribution.

Ömer Hükümdar, Cihan Filiz, Anıl Ersoy and Orkun Bunsuz have performed great effort to provide reliable and useful results for the experimental studies and numerical modelling. Without their energy it wouldn't be possible to complete this journey. I express my sincere gratitude to them for their devoted and serious work.

I am grateful to my children Berkin and Zeynep, and my better half Özge, who are my greatest motivation for the success of this adventure.

TABLE of CONTENTS

LIST OF ABBREVIATIONS AND ACRONYMS

<u>Abbreviations and Acronyms</u>		**<u>Explanations</u>**
ϵ	:	Strain
σ	:	Stress (Von Misses)
ABS	:	Acrylonitrile butadiene styrene
E	:	Elasticity Modulus
g	:	Gravitational acceleration
H	:	Height
JC	:	Johnson-Cook
Kg	:	Kilogram
M	:	Mass
OEM	:	Original Equipment Manufacturer
PA	:	Polyamide
PE	:	Polyethylene
PMMA	:	Poly methyl methacrylate
PP	:	Polypropylene
S	:	Second

LIST OF FIGURES

LIST OF TABLES

1. INTRODUCTION

An overview about automotive applications of high performance plastic materials, indicates that the use of plastic materials in vehicles has increased over the years. According to the research, while 3% of the weight of the vehicle was plastic in 1970, this ratio reaches 10% by 2006 [1]. Vehicle weight reduction is known to be a simplest and cheapest solution to reduce energy consumption. It is estimated that approximately 10% reduction in vehicle weight will result in a 6% to 8% reduction in fuel consumption [2]. Along with the reduction in fuel consumption, each 1 kg reduction in vehicle weight has the potential to reduce carbon dioxide emissions by 20 kg [1]. Plastics are filling more volume in vehicle composition day by day and being indispensable components of the automobile architecture due to mass and cost reduction advantages.

Plastics, used in automobile production are developed to meet certain needs and fulfil functions. Vehicle components are exposed to various mechanical loads and environmental conditions. Several types of polymers are used in the automotive industry to meet requirements. Examples to these polymers are; polyamide (PA), polypropylene (PP), acrylonitrile butadiene styrene (ABS), polycarbonate (PC), poly-methyl methacrylate (PMMA) [3].

Compared to other elastomers, PP has remarkable cost and mass advantages. A neat PP has a density of 0.90 g/cm^3 [4]. Crude oil and energy consumption due to PP production is relatively low compared to other polymers [5]. Less energy and oil consumption needed for production of polyethylene (PE), however it provides lower mechanical characteristics. ABS records better mechanical strength than PP in many respects. However, the price of ABS is higher than PP, since its production cost is higher due to energy consumption [6]. A study indicates that in 2016, PP was the most demanded polymer with 26% in the volume distribution of polymer demand worldwide [7]. Parallel to this, also in automotive industry PP is widely used too. A study that references the data of the benchmark company A2mac1.com has revealed that approximately 40% of the total polymers used in Diesel, HEV and gasoline passenger cars are PP [3]. Tendency is to use PP based material with additives to improve stiffness, strength, thermal resistance, shock, scratch, flammability, UV, weathering. For instance, elastomer modified, mineral filled PP is widely used in bumper fascia. In vehicle architecture, bumpers are considered energy absorbers, so they are expected to have high toughness values. Therefore, as stated in the research, 90% of the bumpers used in vehicles in Europe are made of PP-based materials [8]. Especially front bumpers are also exposed to stone chipping. Therefore, they are expected to have higher toughness values and higher wear resistance. PP composites are extensively used in front bumper zone where maximum energy absorption is expected. Other vehicle components exposed to stone chipping are rocker panels, door side strips, wheel hoods and under-vehicle protection covers. The primary functions of these parts are to prevent the areas they protect from being exposed to stone load and to prevent corrosion by preventing the coating and paint on them from being worn away.

Neat PP is naturally known to be ductile but due to stiffness, thermal resistance, thermal expansion requirements, it is compounded together with additives such mineral filler, talc which is negatively affecting the toughness. Detail review given in section 1.1 in this thesis study. Developing a product both stiff and tough, is challenging due to this conflict material selection point of view. Other option to ensure product stiffness is increasing the material thickness and optimization of the geometry, however in this option material consumption is greater. Therefore, it is possible to consider this conflict as an optimization problem.

In many sectors, including automotive industry is using recycled raw material. Generally, recycled raw materials are cheaper compared to virgin raw materials. The use of recycled plastic contributes to reducing the product carbon footprint, as it reduces greenhouse gas production by eliminating the oil consumption associated with the production of virgin plastics. Emissions from recycling activities are considered to be less [9]. Automobile manufacturers are also committing on vehicle recycling from their sustainability perspective [10].

The mechanical properties of the products produced with recycled plastic differ from those produced with virgin raw materials. Research on comparison of properties with relevance for the automotive sector in mechanically recycled and virgin polypropylene, has indicated with mechanically recycled PP, Charpy impact strength and elongation at break are reduced [11]. For non-aesthetic components, Tier 1 suppliers are challenged by automobile manufacturers to develop products with recycle materials. Rear axle cover, as an under hood compartment product, is in this category. Along with these boundary conditions, part manufacturers should minimize the stresses that will occur in the part, depending on the loads to which the product will be exposed, during the product development phases.

The rear axle protective cover is developed to prevent the formation of corrosion on the axle by protecting the rear axle from stone load. While the source of the stone for the bumper and door strips is the rear wheel of the vehicle in front, the stones that come to the rear axle protective cover are the ones that get stuck between the front wheel of the vehicle and the road and throw towards the rear of the vehicle. Stones can hit the rear axle cover in two different driving situations: skidding and driving on a gravel road. In the driving situation, since the time it takes for the stone to reach the rear of the vehicle from the front wheel and the distance between the two wheels is short, the minimum collision speed can be accepted as the speed of the vehicle, ignoring its acceleration or deceleration. With this assumption, the driving speed on the gravel road specified in the specifications is more than 15m/s. Therefore, the stone load can be considered as a dynamic load. In the literature, there are studies on design optimization of structures under dynamic load. These studies were mainly carried out for metal-based parts [12]. There is no specific study on optimizing the designs of plastic parts exposed to stone load.

While there are valid fracture models used for metal parts, the applicable fracture models for plastic parts are more questionable. In a study on the impact test simulation of plastic parts, it was observed that there was a difference between the predicted fracture type by numerical analysis and the experimental results [13]. Stone load, which is the subject of the thesis, causes failure together with wear, penetration and similar different failure modes. Moreover, sharpness of the stone is affecting the failure types thus it is not possible to make structural optimization with a single analysis. Approach of the thesis is to have comparative results between different design configuration to optimize the shape for minimum stress and cost with help of FEA and optimization tools.

1.1. Literature Review

Researchers have classified impact response of materials according to various velocities. According to Vaidya (2011), velocities up to 10m/s are defined as low velocity impact, while material response at speeds between 10m/s - 50m/s are defined as intermediate velocity. Impact range of high velocity is 50m/s to 5000m/s, which is also named as ballistic impact. Speeds of 2-5 km/h and above are called hyper velocity. Witness material's behaviour is similar to the liquid. Low velocity (large mass) impact arise from piece drop and simulated with ball drop tests and pendulum tests; (Charpy impact test or Izod impact tests). Collisions caused by small calibre projectiles are in high velocity regime. In the case of a high velocity impact, the shock wave travels faster in the direction of the target plate thickness. Boundary conditions may be negligible because it happens so fast, the collision is complete before the shock wave reaches the fragment boundary. Low velocity impact result in a quasi-static response. Intermediate velocity impact includes characteristics of both low and high velocity impact [14]. Cantwell and Morton (1991) also defined low speed velocity impact limit as 10 m/s. According their approach, low velocity impact behaviour could be assessed with pendulum tests (Charpy and Izod) and instrumented drop weight impact. For high and intermediate velocity impacts, Cantwell and Morton (1991) proposed Hopkinson-bar technique, which is a dynamic tensile testing methodology and it is instrumented with strain gages [15]. There are also researches, proposing impact type classification according to damage incurred [16]. Within the scope of this thesis, in experimental studies low velocity impact loading applied through target panel and intermediate velocity impact loading applied in computer simulations. In two different setups, impactor shapes are different however failure mode in both tests are similar; crack initiates in the target point, boundaries are not adversely affected.

There are many studies on the analysis of dynamic collision problems with experimental, numerical and analytical methods. The effects of impactor type, orientation of the target panel, material, thickness and similar parameters on material behaviour were investigated by researchers. These studies enable design optimization of structures under dynamic loading.

Kurtaran H. et al., (2003) have performed penetration simulations of hemispherical bullet on military vehicle door with various speeds from 500m/s to 1500m/s. FE simulations are conducted using plastic kinematic and Johnson–Cook (JC) material models. [12] In an extensive research, Kurtaran H. et al., (2003) successfully performed an optimization via Ansys LS-Dyna software, for best panel thickness and orientation leading least penetration and lightweight design [17]. However, this study does not consider the varying impactor shape and material model is less appropriate for polypropylene. In 2011, Omar et al., experimentally analysed compressive response of PP, PE and PC for different strain rates using a Hopkinson pressure bar. According to this experiment polypropylene has highest strain rate dependence in static region. In dynamic region, with higher strain rates, Yield Strength of material is increasing without significant change in Elasticity modulus [18]. Gebremeskel et al., (2018) compared experimental and numerical studies accuracy with different material models for PP nanocomposites, for intermediate velocity impact regime (~35m/s). Strain rate model of Omar (2011) resulted with accurate results (0.5%) while JC model's accuracy is ~7% [19]. Same research article also highlights effect of thickness to the strain-stress behaviour. For a neat PP specimen, three specimen thickness compared varying from 0.35mm to 1.4mm, and each specimen has different impact strain-stress plots. Thickness increase has resulted in reduced Yield Strength under impact loading. However, in nanoclay addition sensitivity of elasticity module to the thickness become more negligible compared to neat PP [19]. In rear axle cover case, thickness range is 1.5mm to 3.5mm. Study of Shokrieh et al., (2015) also confirms that slope of strain-stress curve is similar in different strain rates for both neat PP and graphene/PP composites with a tensile test setup [20]. Vaidya (2011) summarized importance of the impactor shape by comparing sharp, ogive and blunt geometries. Impact response from sharp impactor resulted in a smaller delamination area and less energy required to create the failure with the sharp geometries. Daiyan et al., (2010) studied also with different striker geometries and analysed low velocity impact respond of an injection molded polypropylene target plate. In this study two hemispherical and one flat ended striker used. Results show, displacement-force curve and crack type are highly sensitive to the striker geometry [21].

Studies indicate that the shape of the striker has a great effect on the type of fracture. We will perform low velocity impact experiments with sharp impactors to replicate the fracture types that occur in the rear axle cover, localized at the impact point. In addition, we will perform intermediate velocity impact simulation with hemispherical impactors. Because it is known that the geometry of the stones hitting the rear axle cover is different and this situation should be taken into account in the optimization study. The common aspect of the experimental and numerical studies is that conditions similar to the type of fracture seen in the rear axle part will be created in the real situation; crack or stress will be maximized in striking point not in fixation areas. Apart from these valuable studies, no comprehensive study has been found on the structural optimization of a product made with injected polypropylene. Alcock et al., (2006) analysed PP composite fabrics and indicated that specimen thickness is proportional to total penetrative energy, under low velocity impact loading [22]. Fernando and Williams (1980) also pointed out linear relation between thickness and fracture energy in slow rate for a polypropylene [23]. Fernando (1988) followed similar approach for a polypropylene copolymer, with a high rate impact tester, in low velocity regime (5m/s) and confirmed linear relation of fracture toughness with thickness [24]. These studies provide useful information when it is desired to optimize with the response surface method using geometry inputs.

Many researchers have analysed underbody impact. Yong-Ju Chu, (2018) calculated absolute stone speed, they showed vehicle speed, mass of vehicle and tyre speed are increasing the stone speed and the energy [25]. Figure B-1 shows the calculation details of the stone velocity. In this study, for computer simulations, vehicle speed assumed to be equal to relative impact speed. Selected drive speed is 60km/h. Researchers investigated probability of cumulative energy, speed of gravel with similar methodologies. Speed calculations are not verified with physical measurements.

In bumper facia for stone grid velocity is already defined by Original Equipment Manufacturer (OEM) as 145km/h and 60km/h for underbody compartment [26].

In an OEM (BMW) research, test setup created to monitor the gravel speed with cameras. Since experimental velocity measurements are not included, it is predicted that the measurement with the camera could not be performed successfully. A software was used to understand probability of the impact location and detect surface normal momentum of stones at impact. The simulation is in good agreement with physical experiments; physically corrosion occurs at the region of high normal momentum impact, shown by simulation [27]. Figure B1.2 shows the damage probability study. In this research (Gruen, 2015) we understand that stone chipping simulation can be used to identify problems in early stages of the development. It is possible to use a plastic cover to prevent corrosion. Areas that will be exposed to impact load and that are likely to break can be foreseen on this protective cover. Impact simulations for these risk areas can be performed locally.

R.Vadori (2010), used Hyperworks to detect damage probability of single touch on vehicle underbody media. Also defined kinetic energy E_u of re-bounced particle and locally absorbed energy E_a. By creating a plug-in to Hyperworks, they calculated the energy distribution in under body [28].

$$E_u = \frac{1}{2} m_P (1 - \bar{\alpha})^2 v_i^2 \tag{1.1}$$

$$E_a = E_i - E_u = \bar{\alpha}(2 - \bar{\alpha}) E_i \tag{1.2}$$

Figure B.1.3 shows cumulative of absorbed energy and contour plot of the underbody.

Toughness of raw material is being considered as an important factor for resisting impact loading. Extensive researches have been carried out to improve toughness of polypropylene. Researcher Hartl, A. M. (2015) measured positive influence of short glass fibre and talc [29]. According to this research rubber is tended to reduce modulus of polypropylene. Rubber is increasing toughness of PP, but stiffness and strength is reduced. Short Glass fibre increases strength with minimum toughness. In Figure B.4 stress-strain trends in compression and tension of PP-R32 are shown. Also in Figure B.5 Overall illustration of mechanical anisotropy of all materials investigated in terms of tensile E-mod- ulus versus tensile strength are shown.

Jung, W. Y., compared pure Polypropylene Impact copolymer (ICP) with variants of ethylene–octene copolymer (EOC) and talc additives. (2013) With Charpy tests and microscopy observations, they noticed positive impact of EOC and talc on impact behaviour [30]. Table B-1 shows impact strengths of the ICP and ICP blends sample.

Figure B1.1 shows the 3 Transmitted optical stereo micrographs of DN-4PB Charpy impact-tested damage zone at 0 °C for three ICP blends: a neat ICP, b ICP/ 30.

Lehmann, B. (2003) analysed notch toughness of low nano Silicone dioxide filled polypropylene composites. For similar tensile strength, elongation and notch toughness were increased. This shows with nano-SiO2 composites, it is possible to improve toughness without decreasing stiffness and strength [31]. This confirms study of Hartl, A. M. (2015) Rubber is decreasing stiffness and increasing the toughness. In the Figure 6.4 Young Modulus, Tensile Strength, Elongation to break and notched Charpy impact strength of PP and its composites filled with nano-SiO2 (content of nano-SiO2 = 0.84 vol%). nano-SiO2 and EPDM (content of nano- SiO2 = 0.84 vol%, content of EPDM for SiO2/EPD are shown.

Researcher Y. Lin. (2008) analysed impact toughness of annealed polypropylene (PP) nanocomposite containing CaCO3 nanoparticles [32]. For similar tensile strength, elongation and notch toughness were increased.

Nanoparticles can dramatically improve the impact strength of i-PP under certain circumstances. In Table B 1.1, the mechanical and thermal properties of i-PP and nanocomposites with and without heat treatment, is shown.

While typical fillers such as talc, rubber, glass filler has directly related to notch toughness and strength nano-fillers are able to keep initial stiffness and improve notch toughness. In the studies there is no information about the industrial applicability and cost merit of nano-fillers while talc, rubber type fillers' commercial impacts are known.

Researchers indicate that if the tensile testing upon additive usage elongation and strength is inversely proportional and total elongation (elongation at break) and izod / charpy notched impact strengths are proportional.

Researchers used notched specimen in their experiments. However, notch initiation behaviour under loading, resistance to abrasion is not analysed. Studies on un-notched bodies and multi-axial impact behaviour of materials also should be investigated as stones are candidate to remove particle from product with their sharp and abrasive structure, rather than penetrating.

Results of researches with polypropylene are not in conflict. As Lehmann, B. (2003) and Hartl, A. M. (2015) concluded that rubber blends are good to improve toughness with reduction of strength we can conclude that experiments are repeatable.

For its importance, it can be said that the rear axle cover is behind the rear axle. After all, it is a protective cover. With the simulations mentioned in the studies, it can be thought that the stones coming to the cover can be eliminated by changing the geometry of the undercarriage. However, this is not permissible considering the vehicle architecture, ground clearance and aerodynamic loads. For this reason, it is inevitable that the rear axle cover is exposed to stone load. The work that needs to be done is to identify these regions and to carry out design optimization studies.

The intention of the thesis is to optimize the structure with best geometry parameter for minimum cost and stress similar. There are also optimization approaches considering material ingredients as a function. Ghasemi et al., (2016) created response surfaces of elasticity modules, tensile strength and impact strength from different level of PP, talc and graphene [33]. If a feasible result cannot be obtained with structural optimization, we can also include material parameters in the response surface within the scope of this study.

1.2. Contribution of the Thesis

While there are numerous studies exists of analysis of quantifying impact loading on vehicle underbody, no study has been noticed to analyse toughness of covers which are used in this region. Also due to lack of robust fracture, model for plastic parts analysis option is mostly neglected. Purpose of this study is to evaluate the effect of impactor type on impact strength of the product. Even the accuracy of explicit analyses for plastic parts are questionable, if the maximum stress is limited to yield stress in a safe zone, a comparative analysis will be made in order to optimize the internal energy of the product. In this study, different geometries are created with different parameters. Each geometry is analysed separately with FEA software and results will be used to make a surface fitting of stress from thickness and angle parameters. This is a simplification approach to understand behaviour of the product and effect of the parameters. Finally, parameters are optimized with manufacturing and material strength constraints.

1.3. Organization of the Thesis

Section 1 is introduction to the thesis. The engineering problem explained and literature review made in section 1. Impact loading terminology explained; high-low-intermediate velocity impact classification and damage types are listed. Previous studies about underbody gravel distribution analysed. Benefit of FEA analysis and optimization theory discussed.

In section 2, plastic materials classification detailed. Section 3 includes fundamentals of FEA and optimization theory.

Section 4 is separate from the experimental and numerical studies carried out within the scope of the thesis. In section 5, optimum design parameters are calculated from the data obtained in section 4.

Finally, conclusion and recommendation are given in last section.

2. MECHANICAL PROPERTIES OF POLYMERS

2.1. Stress-Strain Relation

Engineering strain-stress behaviour is determined with the tensile tests. P is the applied load at the specimen which has a section of A_0. l shows final length of the part while it is l_0 initially. Engineering stress is $\sigma = \frac{P}{A_0}$, Strain is $\varepsilon = \frac{l-l_0}{l_0}$ (Sittichai, 2001). [34]. The general acceptance in solving structural engineering problems is that the stress-strain relationship is independent of the part geometry. Thus, the unit displacement of the material under stress can be calculated.

2.2. Material Regions

The elastic behaviour of the material can be defined as the geometry being the same when the load is applied and when it is removed. The region where the material exhibits this behaviour is called the elastic region. In elastic region stress and strain has linear relation. End of this linearity is defined as proportional limit. This region is called elastic region [35].

Yielding region starts once stain is in the proportional to stress limit. In this region, specimen is deformed permanently, and elongation increases without increase on the stress and $l > l_0$.

Strain hardening region is also called as work hardening. Strain hardening is strengthening specimen by deformation. Strain hardening region is limited with yield point and ultimate stress [34].

Necking region is between strain at ultimate stress to rupture. Cross-section of specimen is decreased in necking region. Fracture stress occurs while specimen reaches maximum elongation before rupture. Stress-strain, material behaviour regions and terminology can be seen in Figure 2.1 below. This curve is mainly valid for metallic materials. Yielding or strain hardening is not that visible for all polymers. The typical stress strain curves are given in Figure 2.3.

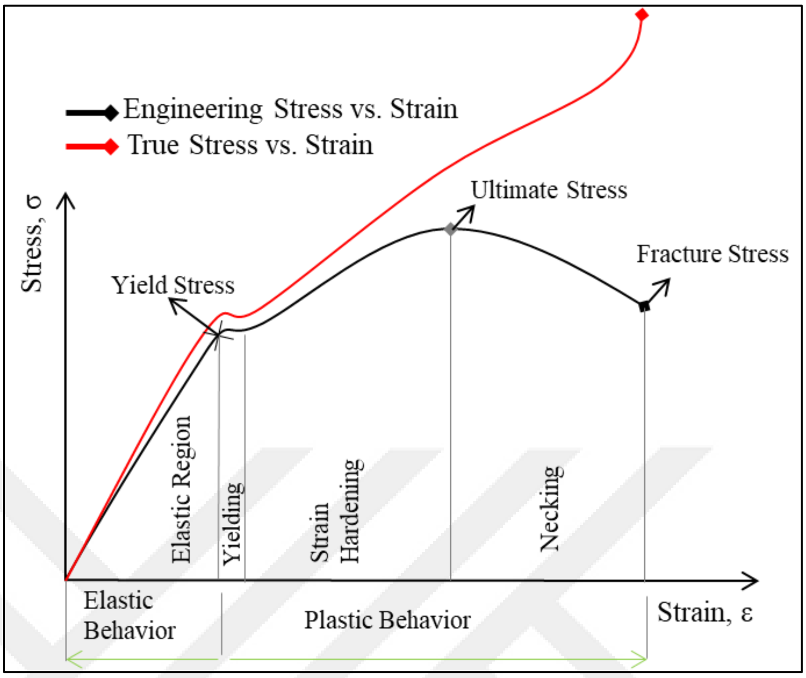

Figure 2.1: Stress-Strain, material behaviour regions and terminology.

2.3. Toughness

Toughness is definition of total energy per volume to break the material. Geometrically it is the area under the curve of stress vs. strain. In elastic region if the curve is integrated prior to yield region this is called modulus of resilience. (Patel et al., 2009) [36].

Toughness graphic is shown in Figure 2.2 below; In Figure 2.3 stress-strain behaviour of polymers is explained.

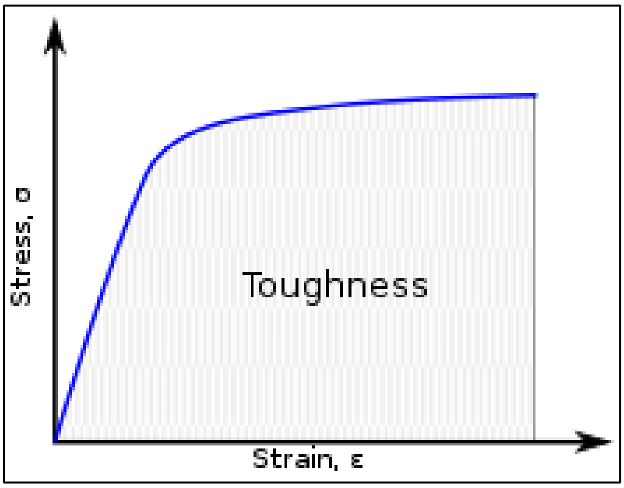

Figure 2.2: Toughness (Wikipedia). [37]

$$\frac{energy}{volume} = \int_{0}^{\epsilon_f} \sigma \, d\epsilon \tag{2.1}$$

Here ϵ is strain, ϵ_f is strain upon failure, σ is stress.

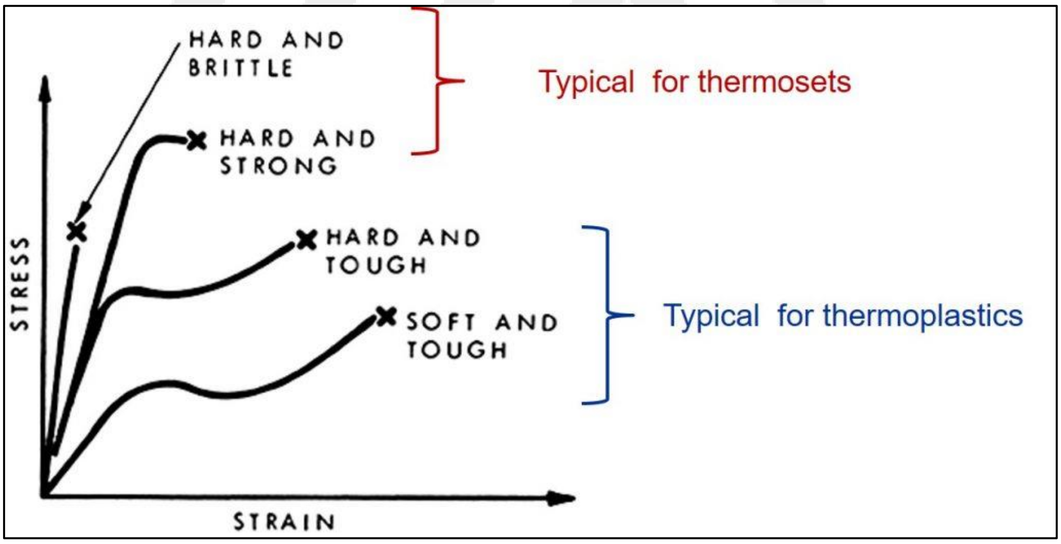

Figure 2.3: Stress-Strain behaviour of polymers [38]

2.4. Elasticity Modulus

Elasticity modulus or Young modulus is the slope of stress strain curve in linear region where material shows elastic behaviour. Strain is expressed as a percentage. Thus, unit of elasticity modules is MPa. Generally, elasticity modulus is in good agreement with flexural modulus.

2.5. Flexural Modulus

Flexural modulus is widely used for testing brittle thermoplastic or thermoset materials such polypropylene with glass filler or polyamide. Flexural modulus values of materials are measured with setups such as three-point test and four-point test. In the three-point test of a rectangular specimen with an isotropic material, flexural modulus E_{bend} is as given in equation 2.2 where w and h are the width and height of the beam, I is the second moment of area of the beam's cross-section, L is the distance between the two outer supports, and d is the deflection due to the applied load F at the middle of the beam. Maximum displacement in three-point test (d), is given in 2.3. d is displacement along load direction, h is vertical dimension of specimen vs load direction, w is width of the specimen in lateral axis. Flexural modulus is also called as bending modulus.

Flexural test is useful to anticipate maximum deflection requirements with a linear-static analysis per OEM requirements which limits the amount of deflection under a specific load.

$$E_{bend} = \frac{L^3 F}{4wh^3 d} \quad (2.2)$$

$$d = \frac{L^3 F}{48IE} \quad (2.3)$$

Flexural modulus figure is shown in Figure 3-4 below;

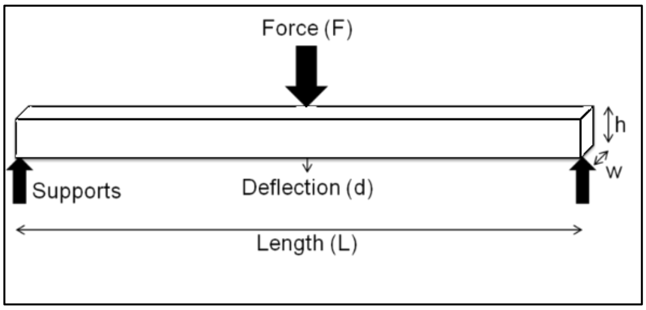

Figure 2.4: Flexural Modulus (Zweben, 1979) [39].

2.6. Engineering Materials

Engineering materials are classified as: (Tong, 2019) [40].

- Metallic Materials
- Polymers
- Ceramics
- Composites

Plastics comprises long chain of polymers. Plastics can be synthetic or partially synthetic, organic compounds which are formable.

Polymer is a chemical specie of very high molecular weight made up from many units of low molecular weight, linked together covalently. A compound used to make a polymer (and from which the polymer's unit arises) is named a monomer. As an example; polyethylene consists from many ethylene monads, CH2CH2, which are covalently bonded to each other to form long-chain molecules from thousands of ethylene units. The name polyethylene stems from the name of the monomer (ethylene) plus the prefix poly-, means "many." In below; Figure 2.1. created to point out the place of polypropylene in the classification of engineering materials.

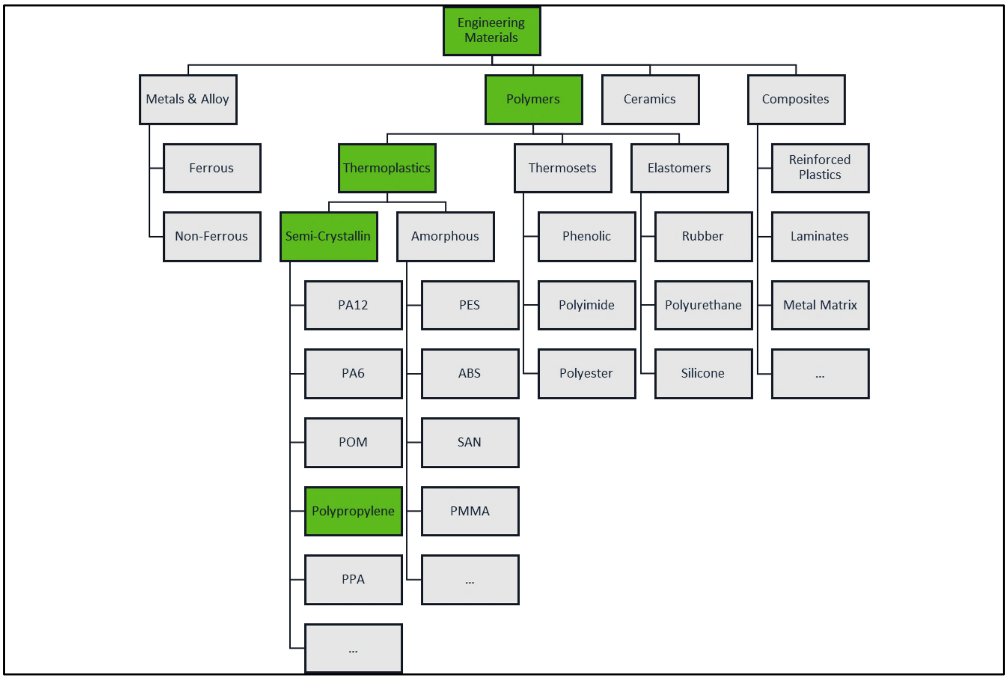

Figure 2.5: Polypropylene place in the classification of engineering materials. (Reproduced from (Tong, 2019))

2.6.1. Classification with Origin of Source

Polymeric materials are classified with their origin of source as; (Khalil et al., 2013).

- Natural polymer
- Synthetic polymer
- Semi-synthetic polymer

Organic polymers contain oxygen, nitrogen atoms, primarily carbon. Inorganic polymers contain silicon, germanium, boron, phosphorus on the main chain instead of carbon. In inorganic polymers, the bond energy of the elements on the main chain is higher than those in organic polymers. Therefore, although organic polymers are used more widely, inorganic polymers have higher heat and mechanical durability. (Khalil et al., 2013).

While rubber is an example for natural polymers, nylon fibre and polyethylene synthetic and vulcanized rubber are in the family of semi-synthetic polymer due to the fact that they are artificially modified from natural polymer in laboratory conditions.

2.6.2. Classification with Structure

It is possible to classify polymers with their structure in three groups; (Khalil et al., 2013).

- Linear,
- Cross-linked,
- Branch chain.

Linear polymers are comparative in structure to a long straight chain which indistinguishable connections associated with one another. The monomers in these group are connected together to shape a long chain. These polymers have high degree of melting point and high density. Poly-vinyl chloride (PVS) is a common example to linear polymers.

Cross-linked polymers or Network Polymers consists of monomers where they are engaged each other to form a network which is three dimensional. Cross-linked polymers have high tensile strength and lower elongation. Melamine is an example for this category. (Wilson, Richard & Pfohl, William. (2000)) [41].

The structure of branch chain polymers resembles branches starting indiscriminately focuses from a solitary straight chain. Monomers join to shape a long straight chain with some stretched chains of variable lengths. Due to presence of these branches, the polymers are not firmly pressed each other. The density and the melting point of these polymers is low. Low density polyethene (LDPE) is an example for this category. (Wilson, Richard & Pfohl, William. (2000)).

2.6.3. Classification with Molecular Forces

Polymers are classified into four types depending on molecular strength;

- Elastomers,
- Thermoplastics,
- Thermosetting polymers,
- Fibres.

Van der Waal’s forces hold long-chains of thermoplastic polymer together. Thermoplastics behave softer with heating and harder after cooling. As thermoplastics don’t include cross bonds they are easily processed by heating. Polystyrene (PES) or PVC are examples for this behaviour.

Thermosetting plastics are semi-fluid in nature, they have low molecular masses. With heating, they initiate cross-linking between chains and become strong and infusible and they create a three-dimensional construction. This is not a reversible reaction in the nature. Bakelite is a synthetic example of thermosetting polymer, it is used for insulating electricity (W. A. Zinzow and Thomas Hazen, 1935) [42]. Classification of polymers is shown in the Figure 2.6 [43].

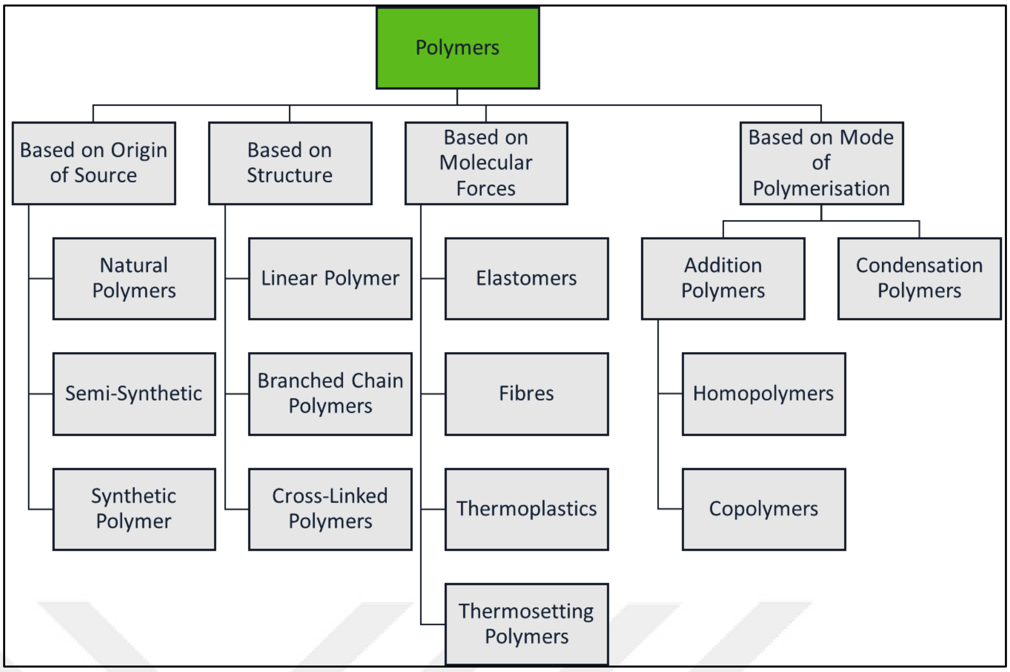

Figure 2.6: Classification of polymers. (Reproduced from Khalil et al., 2018).

It is possible to classify thermoplastics by their technical properties such as hardness, density, temperature and resistance. Thermoplastics can also be classified based on their physical structure in two types;

- Amorphous,
- Semi-crystalline

Figure 2.7 shows widely used thermoplastics classification of plastic according to their physical structure This classification method has an advantage compared to others due to mainly upon the underlying molecular structure of the polymers. Thermoplastics can become liquid with heating. Because of requiring remarkable ordering of high coil macromolecule in liquid state, thermoplastics don’t crystallize with cooling. Those which crystallize invariably do not form perfectly crystalline materials but instead they are semi-crystalline with both crystalline and amorphous regions. The crystalline phases of such polymers are characterized by their melting temperature Tm. Above melting temperatures, polymers can be converted into artefacts by conventional polymer-processing techniques such as extrusion, injection moulding and compression moulding. Many of thermoplastics are, completely amorphous and they are not able to crystallize, even with annealing [43].

Glass transition temperature T_g is a characteristic of amorphous polymers at which these polymers transform from the glassy (hard) state to the rubbery (soft) state. Glass transition corresponds to the initiation of chain motion. Prior to glass transition temperature, the polymer chains are not able to move and their position is locked. Both melting temperature and glass transition temperature increase with chain stiffening and increasing forces of intermolecular attraction.

PP is primarily used due to its cost advantage. There are wide range of applications in automotive, especially it is the main choice due to ductile behaviour. Typically, thermosets have bigger strength compared to thermoplastics while thermoplastics are tougher. Thermoplastics pyramid can be seen in Figure 2-3 below [44];

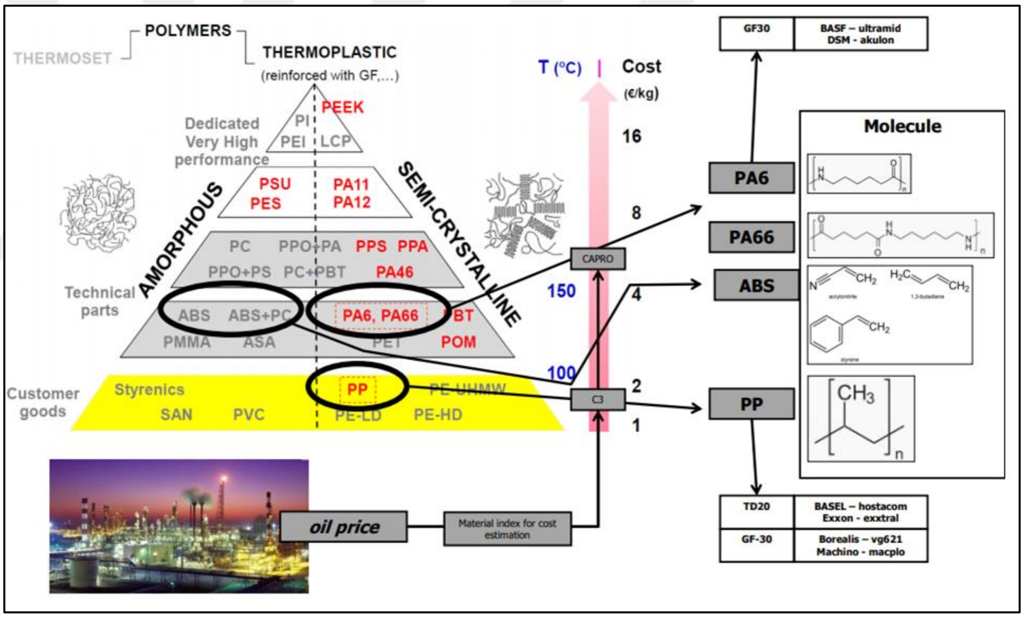

Figure 2.7: Thermoplastics pyramid (Novares, 2019)

3. FINITE ELEMENT METHOD and OPTIMIZATON THEORY

3.1. Finite Element Method

Finite Element Analysis (FEA) is a numerical analysis methodology to solve engineering problems of complex structures. In Finite Element Method [45], complete structure is separated in smaller elements with specified sizes and shapes. Elements are connected with nodes and with that equation sets obtained. The finite element method is a systematic procedure of approximating continuous functions as discrete models. This discretization involves finite number of points and subdomains in the problem’s domain. The values of the given function are held at the points, so-called nodes. The non-overlapping subdomains, so-called finite elements, are connected together at nodes on their boundaries and hold piecewise and local approximations of the function, which are uniquely defined in terms of values held at their nodes. The collection of discretized elements and nodes is called the mesh and the process of its construction is called meshing [46].

3.2. Explicit Dynamic Finite Element Theory

Explicit dynamic finite element analysis is a widely used method in recent years for modelling the behaviour of real structures under quasi-static or dynamic loading in computer environment. The method is one of the most important tools of Computer Aided Design/Engineering (CAD/CAE) today. Thanks to this method, the prototype development process is transferred to the computer environment, accelerated and the cost is reduced [47].

LS-DYNA and Ansys Explicit Dynamics use a finite element formulation based on displacement, Lagrange, central differences, to capture the nonlinear behaviour of structures [48]. This formulation is based on Cauchy's first law of motion and the virtual work principle in determining the potential energy equation. The potential energy equation is primarily discretized in space with a finite element mesh and shape functions. It is then discretized over time using the explicit central differences method to extract its dynamic equivalents [49].

3.3. Time Step Criterion

Selection of time steps is critical in explicit dynamic finite element analysis. A large time step makes the solution indecisive. Small time step leads to negative consequences in terms of computational cost. Therefore, the time step must be determined correctly. The critical time step must satisfy the stability conditions of the explicit method. The Courant criterion tells each time step to be chosen small enough to avoid crossing over more than one element [50].

$$\Delta t_e = \frac{l}{c} \tag{3.1}$$

In formula (3.1) ; Δt_e defines critical time step, l is critical length and c is wave velocity. For one sized elements, it is calculated as (3.2). While E is elasticity modulus, ρ is density of the material.

$$c = \sqrt{\frac{E}{\rho}} \tag{3.2}$$

With help of (3.1) and (3.2) time step for beam element obtained as (3.3)

$$c\Delta t_e = l.\sqrt{\frac{E}{\rho}} \tag{3.3}$$

3.4. Comparison of Explicit and Implicit Methods

Although the explicit theory is introduced in this section, it will be useful to explain the difference between the implicit method and the implicit method. Thus, it will be clarified which method will be more suitable for solving which type of problems. Software such as ABAQUS, NASTRAN are the leading programs that perform finite element analysis with the implicit method. This method is more suitable for solving static and quasi-static (low speed dynamic problems). Explicit method (LS-

DYNA, RADIOSS, DYTRAN, PAM-CRASH, ABAQUS/Explicit, ANSYS Explicit Dynamics) is mostly used in solving dynamic problems as stated in the chapter.

- While implicit method is dedicated to static problems, explicit solutions are more suitable for dynamic, nonlinear problems.
- In implicit methods, inertia effects are not in consideration. Explicit solution uses inertia inputs ([C] and [M]).
- For implicit methods, average acceleration and displacements are calculated in $t = \Delta t$ time point:

$$\{u_{t+\Delta t}\} = [K]^{-1} = \{F^{a}_{t+\Delta t}\} \tag{3.4}$$

In explicit solutions accelerations are calculated for a time point.

$$\{a_t\} = [M]^{-1}.([F_t^{ext}] - [F_t^{int}]) \tag{3.5}$$

- In implicit solution, in case nonlinear solutions, there are convergence issues while it is simple to solve nonlinear problems in explicit solution without any convergence issue.
- Implicit solutions are efficient expect when Δt is supposed to be small, in explicit solutions integration time step has to small [51].

3.5. Optimization of Engineering Design

Optimization is defining ideal design parameters that gives maximum or minimum of objective function, while respecting the constraint [52]. The design of a system can be formulated as problems of optimization in which a performance measure is optimized while all other requirements are satisfied [47].

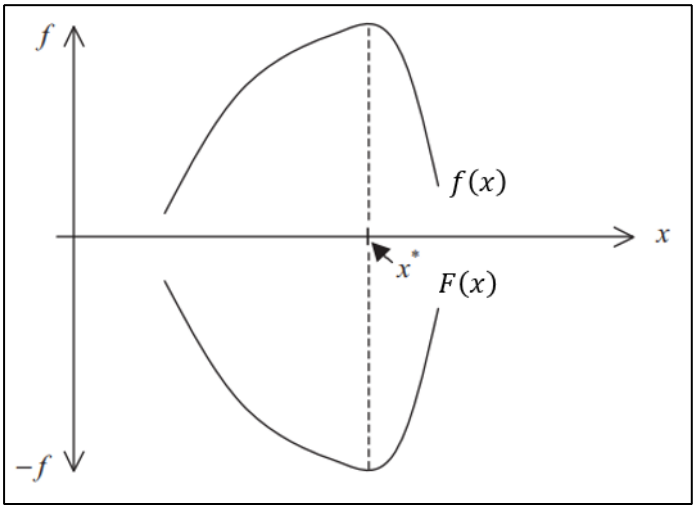

Figure 3.1: Maximization and minimization functions.

General design model solves only minimization problems. There is no restriction as maximization of a function f [47]. To solve this maximization problem, minimization problem is described as $F(x) = -f(x)$. For graphically explaning, one variable function is shown in Figure 3.1. In this graphic $F(x)$ is transformed from $f(x)$ function. While $F(x)$ is minimum at x^*, maximum value of $f(x)$ is found at the same point. It is clear from the Figure 3.1 that $F(x)$ is reflection of $f(x)$ over x axis [52].

Optimum design is the determination of the design parameters (material, geometric dimensions, shape and topology) of the model in a way that will provide the desired design criteria values (weight, strength, thermal, etc.). In the design process, there must be one or more criteria to be done at least or at most.

Commonly used design criteria (for structural engineering):

- Weight: It is attempted to be reduced,
- Stress: It is attempted to be reduced,
- Fatigue life (occurs in case of repeated load): It is attempted to be reduced,
- Uniform temperature distribution,
- Natural frequency: It is tried to be increased,
- Buckling load: It is tried to be kept under the critical load.

In order to meet the criteria mentioned above, some parameters in the design must be changed. Parameters that need to be adjusted are called design variables or design parameters [29].

Commonly used design parameters:

- Material modulus of elasticity,
- Thickness,
- Geometric dimensions: width, height, height,
- Cross-sectional area,
- Hole radius,
- Rounding radius.

For a realistic design, the dimensions must be limited. All restrictions placed on a design are collectively called constraints.

Examples of design constraints:

- Weight ≤ 500 kg,
- $\sigma_{max} \leq \sigma_{yield}$,
- Fatigue life ≥ 1000 (repeated cycle),
- $P_{critical}$ ≥ 500 N,
- 1^{st} Natural frequency ≥ 100 Hz.

A brief classification of Optimization methods according to J.Arora is:

- Optimization Methods
  - Optimally Criteria Methods (Indirect Methods)
- Constrained Problem
- Unconstrained Problem
  - Search Methods (Direct Methods)
- Constrained Problem
- Unconstrained Problem [47]

There are wide range of optimization approaches. In this section only a few candidate methodologies will be explained.

3.6. Numerical Solutions of Multi-Variable Unconstrained Optimization Problems

Numerical optimization methods are based on step-by-step correction. The estimated optimum is iteratively corrected (step by step). At each step, the new (adjusted) optimum value $x_{i+1}$is found by adding the correction amount Δx to the old value x_i:

$$x_{i+1} = x_i + \Delta x \tag{3.5}$$

In numerical methods, the correction amount Δx is calculated differently according to each method. The common method is to calculate the correction amount Δx by dividing it into two different products such as $\Delta_x = \alpha_i * S_i$ Here, S_i is the direction that decreases the value of the function, and α_i is the step length that gives the minimum value of the function in this direction. In this case, the corrected optimum value in the new iteration.

$$x_{i+1} = x_i + \alpha_i S_i \tag{3.6}$$

It is expressed as in the following sections, the calculation of the direction vector S from the term in the correction amount is explained.

Conjugate Gradient Method

The conjugate gradient converges to the optimum point using the slope of the endpoint. For this reason, it converges faster than the steepest descent. Initially an estimation should be done.

$$S_{i+1} = -\nabla f_{i+1} + \beta S_i \tag{3.7}$$

$f(x) = x_1^3 + 3x_1x_2 + 4x_2^2 \rightarrow min$ asked.

$x_1^{(0)}=1$ ve $x_2^{(0)}=1$ are initial estimations.

$x_1^{(1)} = x_1^{(0)} + \alpha S_1$, $x_2^{(1)} = x_2^{(0)} + \alpha S_2$ as given in (3.7) and,

$$S = -\nabla f(x^{(0)}) = \begin{Bmatrix} S_1 \\ S_2 \end{Bmatrix} \tag{3.8}$$

$$S = -\nabla f\left(x^{(0)}\right) = \begin{Bmatrix} \dfrac{\partial f}{\partial x_1} \\ \dfrac{\partial f}{\partial x_2} \end{Bmatrix} = -\begin{Bmatrix} 3x_1^2 + 3x_2 \\ 3x_1 + 8x_2 \end{Bmatrix} = \begin{Bmatrix} -6 \\ -11 \end{Bmatrix} \tag{3.9}$$

From (3.8) equation (3.9) is obtained.

First iteration should be as;

$$Sx_1^{(1)} = 1 - 6\alpha,\ \ x_2^{(1)} = 1 - 11\alpha \tag{3.10}$$

To realize first iteration, α value should be defined. A new equation is given as below with single variable as shown in (3.11).

$$f(x) = (1 - 6\alpha)^3 + 3(1 - 6\alpha)(1 - 11\alpha) + 4(1 - 11\alpha)^2 \tag{3.11}$$

Candidate solutions to solve such polynomial function are;

- Equal internal search,
- Section Search,
- Golden Section,
- Parabolic interpolation,
- Other root analyses methods.

3.7. Multi-Objective Optimization

Once there are multi-objectives, there are two main approaches;

- Considering 2nd and 3rd objectives as constraints.
- Converting the composite objective function from multi-objective optimization to single-objective optimization using weighting coefficients [53].

$$f = w_1 f_1 + w_2 f_2 + w_3 f_3 + \ldots + w_n f_n \rightarrow min \tag{3.12}$$

The weighted sum method is one of the multi-objective optimization methods. In weighted sum method, weight of the objective function is assigned by decision maker. However, as different objective function can have different magnitude, the normalization of objectives is required to get a Pareto optimal solution consistent with the weights assigned by the decision maker. [54] Where sf_i is the normalization factor and equal to average of each objective function, weight sum method is given as in (3.13) [55].

$$f = \frac{w_1 f_1}{sf_1} + \frac{w_2 f_2}{sf_2} + \frac{w_3 f_3}{sf_3} + \ldots + \frac{w_n f_n}{sf_n} \rightarrow min \tag{3.13}$$

4. EXPERIMENTS and NUMERICAL ANALYSES

In this chapter, experiments and numerical analyses performed. In intermediate velocity impact analysis, the striker's mass is an important input. The mass of the stone is in a linear relationship with the loads to which the part will be subjected during the collision. For this reason, a sampling study was carried out on a gravel road, taking into account the size of the stone specified in the specifications. Figure 4.1 shows examples from sampling study. The selection of dimensions was carried out according to the OEM specification [26]. The gravel sections of the test track are paved with two types of stones. Since small particles are less likely to cause damage, the sizes of large gravels (10mm-14mm) were sampled.

Geometry and weights of the stones were examined. The weight used in the numerical analysis was determined as 5g, taking into account the average values.

- 2/6 (quantity: 900 kg i.e. 640 g / m^2 ± 160 g / m^2) and
- 10/14 (quantity: 6,900 kg i.e. 4.9 kg / m^2 ± 1.2 kg / m^2)

As seen in Figure 4.1, while some parts of the stones are sharp, those with blunt or hemispheric geometry have also been observed. In section 1.1, it was discussed that intention is to initiate a localized crack in the hit point of target plate to reproduce similar failure in vehicle tests. To realize that, it is decided initially using a large mass impact test physically with sharp impactors. Following this, numerical analyses will be performed to create a localized stress in hit point from spherical impactors.

Figure 4.1: Gravel Sampling

4.1. Mechanical Requirement of the Cover

Resisting to deflections and shocks are two main mechanical criteria for rear axle cover. Static loads, represent aerodynamic force during cruise. Under this loading condition, deflection of the product is asked to be limited to avoid contact with environment parts as it could cause vibration and noise. In the scope of the thesis this requirement is not analysed. Resisting to shock performance is validated with road tests and external material tests.

While choosing the material, the toughness and stiffness constraints of the product should be taken into account. However, many additives cannot improve these two values simultaneously. For instance, talc additive increases strength and elastic modulus, density, raw material cost, while toughness, elongation at break is decreased.

4.1.1. Strength and Deflection Requirements

An underbody cover is expected to deform maximum 6mm and stone grid is allowed to deform maximum 3mm. In below, Figure 4-1 shows the deflection requirement for underbody application.

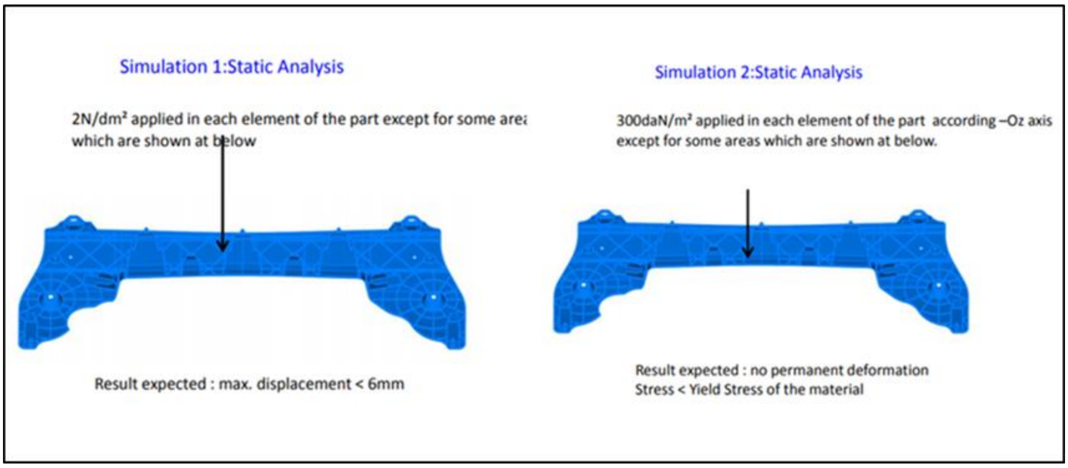

Figure 4.2: Deflection requirement for underbody application.

Also; in the Table 4-1 the resistance to deflection is given;

Table 4.1:Resistance to deflection.

Requirement	**Test Method**	**Criteria requirement**
The part must not damage surroundings parts. No alteration of the assembly part/technical surroundings.	By calculation According to the test $6.11of the specifications 31-07-xxx applied on a grid fitted on radiator.	Maximal calculated deflection allows to keep the integrity of the cover and its fixations. The resulting gap with the environment at least 3mm, under application of the pressure field provided by OEM (corresponding to air speed max)

4.1.2. Impact Requirements

The resistance of the vehicle to the gravel road condition is checked by road tests. The number, size and frequency of stones in the gravel area of the track where the vehicle will be tested are specified by the vehicle manufacturer in the specifications. 37/03 002 / B ‘RESISTANCE AU GRAVILLONNAGE SUR PISTE’ of RSA describes the physical road test with defines size of gravels. 2 types of gravels are defined:

- 2/6 (quantity: 900 kg i.e. 640 g / m^2 ± 160 g / m^2) and
- 10/14 (quantity: 6,900 kg i.e. 4.9 kg / m^2 ± 1.2 kg / m^2)

50 times acceleration is needed from initial velocity=0 km/h to 70km/h and 500 passages from gravel area beginning with 60km/h with acceleration to 80km/h in the zone.

In these conditions a single vehicle is in the parkour and source of impactor is front wheel. Per specification, for numerical analyses, relative impact speed is selected as 60km/h.

4.2. Physical Impact Testing on a Polypropylene Plate

In order to understand the different phenomena of rupture it is considered to use two main types of impactors with different tip in this study.

- Sharp impactor with conical tip
- Non-sharp impactor with spherical tip.

Assumption: During product design optimization subject to minimum absorbed energy, we can find an angle value for the wall that touches to the impactor considering impactor is rigid and wall is deformable, and collusion is partially inelastic, perpendicularity is proportional to absorbed kinetic energy by the wall. Meanwhile if the impactor is sharp, impacted area is more punctual and less energy is needed to break the part and amount of sharpness is greatly important. In this study physical tests performed to evaluate the relation with the angle and the absorbed energy.

4.3. Test with Sharp Impactor

Three types of sharp impactor are defined initially in order to evaluate effect of conicity and flat size at tip. Type A has 1mm flat tip with 80° conicity. Type B has 1mm flat area with 40° conicity, Type B2 has Ø1mm ending without any flat area.

Type C has 3mm flat area with 40° conicity and Type C2 has Ø3mm ending without flat area as given in Figure 8-1. In Figure 8-2 images from impactor are shown.

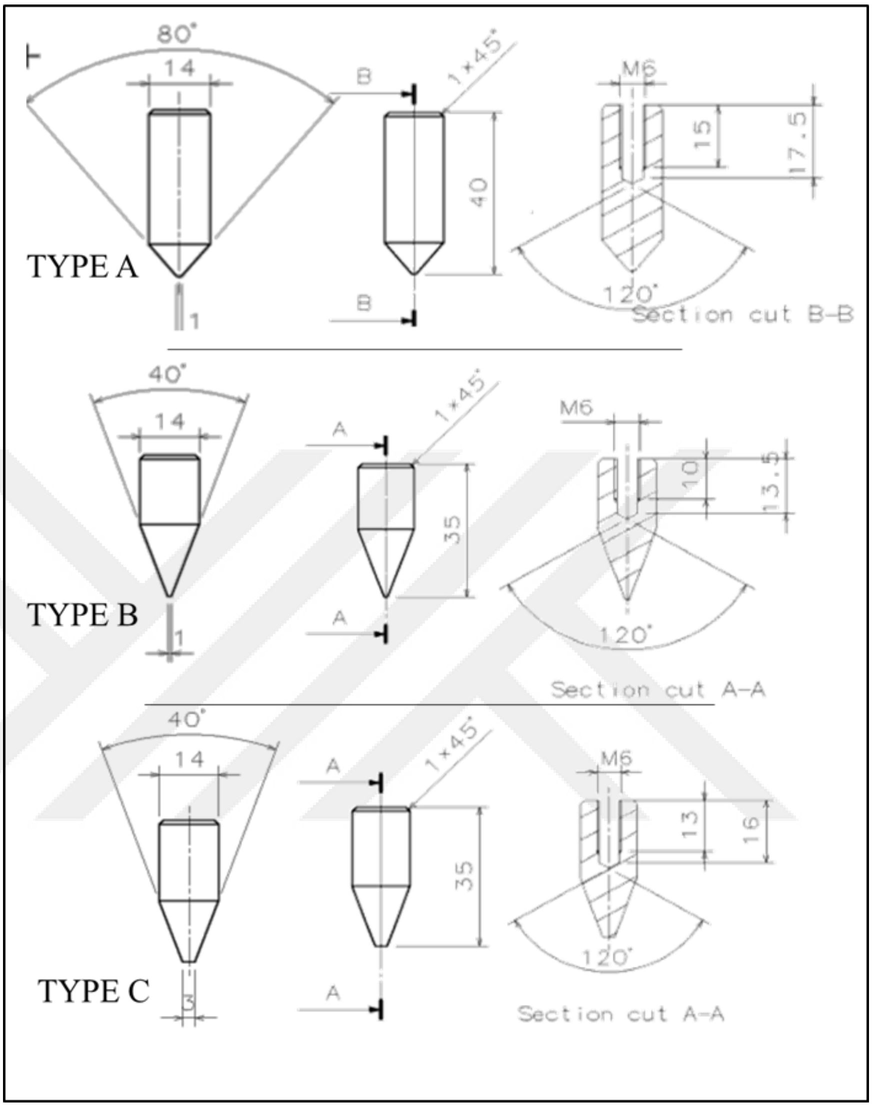

Figure 4.3: Impactor definition.

Figure 4.4: Images of impactor.

A test bench (Figure 4-5) has been manufactured to be able to fix plate reproducibly. The bench also allows to change orientation against vertical impact loading. It is also possible to add support material behind plate which supposed to be broken.

Impactors tip profiles are specified and mass is adjustable with additional mass. Loading assured with gravity constantly from 50cm. Distance at break point is adjusted with several tests and repeated after breakage and reported where crack initiates. Following the height detection, energy to break the part is noted with the below formula.

$$m * g * h = kg * \left({}^{m}/_{s2}\right) * m \; (Joule) \tag{4.1}$$

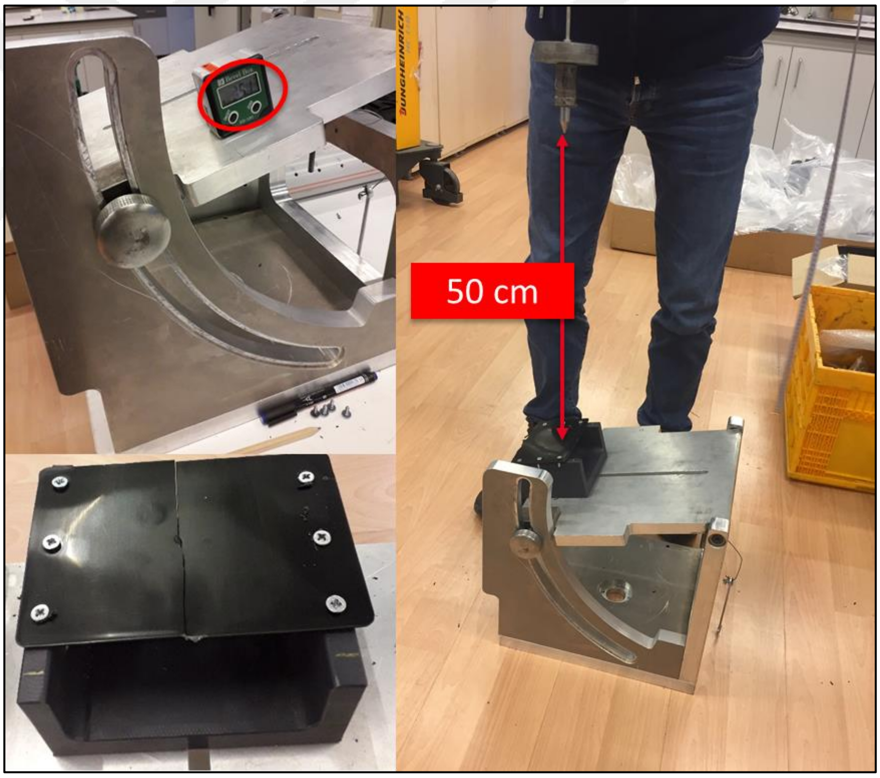

Figure 4.5: Test bench.

Plate size is 150x100mm wide and thickness is 2mm. Selected raw material of the plate is a recycled polypropylene without talc and mineral filler (<5%). In Figure 4-6 definition of plate, angle and support clearance are shown.

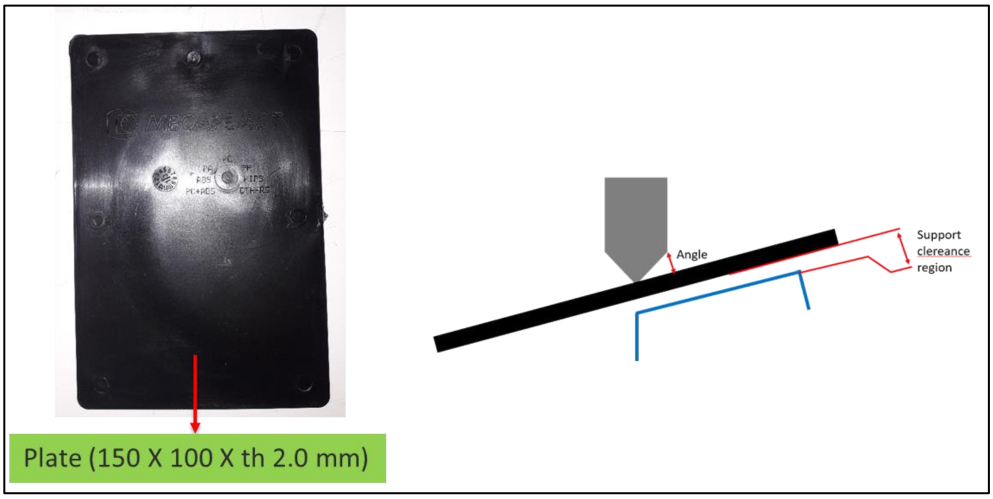

Figure 4.6: Definition of plate, angle and support clearance.

Angular orientation of the target plate is adjustable as given in in Figure 4-7. Test bench allow 90° rotations, however due to clash of target plate additional mass behind impactor (Figure 4.8), minimum angle is defined as 45°.

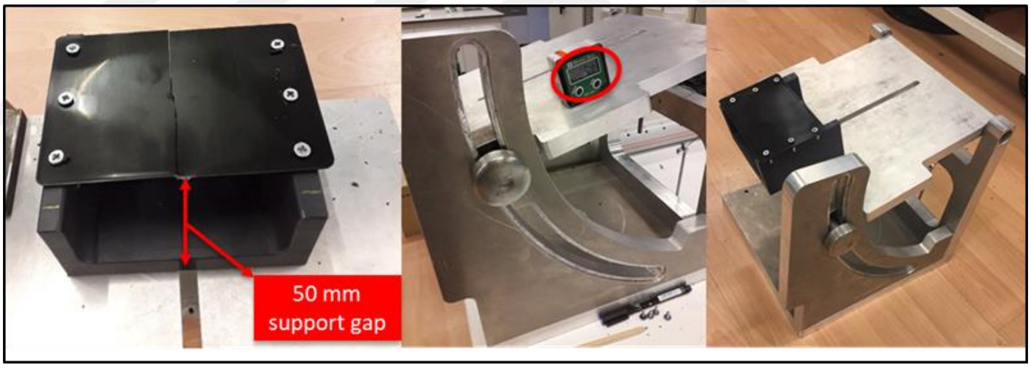

Figure 4.7: Test 1-1 Set up.

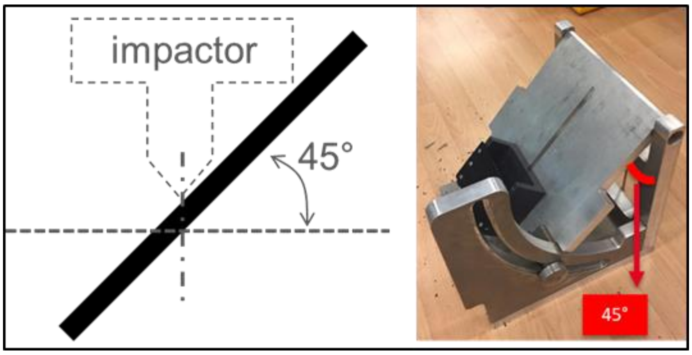

Figure 4.8: Test setup with <45°.

Test results are given in Table 4.2, Table 4.3, Table 4.4, Table 4.5 and Table 4.6.

Table 4.2: Test Results 1.1 – 90° without support Type A, Type B, Type C.

Thickness (mm)	Ball Type	Angle (°)	Mass (kg)	Height (cm)	Support (mm)	Comment	Energy (J)
2	A	90	1,33	50	50	Not broken (NB)	6,523
2	A	90	1,38	50	50	NB	6,769
2	B	90	0.815	50	50	NB	3,997
2	B	90	0,86	50	50	Broken	4,2183
2	C	90	1,52	50	50	Broken	7,4556
2	C	90	1,47	50	50	NB	7,21035

Table 4.3: Test Results 1.2 – 75° without support, Type C.

Thickness (mm)	Ball Type	Angle (°)	Mass (kg)	Height (cm)	Support (mm)	Comment	Energy (J)
2	C	75	1,22	50	50	Not broken	5,984
2	C	75	1,27	50	50	Broken	6,22935

Table 4.4: Test Results 1.3 – 60° without support, Type C.

Thickness (mm)	Ball Type	Angle (°)	Mass (kg)	Height (cm)	Support (mm)	Comment	Energy (J)
2	C	60	1,22	50	50	Broken	5,984
2	C	60	1,17	50	50	Not Broken	5,739

Table 4.5: Test Results 1.4 – 45° without support, Type C.

Thickness (mm)	Ball Type	Angle (°)	Mass (kg)	Height (cm)	Support (mm)	Comment	Energy (J)
2	C	45	1,17	50	50	Broken	5,739
2	C	45	1,12	50	50	Not Broken	5,4936

After 60° testing, we noticed there is no remarkable difference on the energy calculation. It is noticed that impact is disturbed due to lack of sharp contact and additional contacts due to additional mass. For that reason, these results are not used in evaluation.

Table 4.6: Test 1.5 - 60° 0mm support, Type C.

Thickness (mm)	**Ball Type**	**Angle (°)**	**Mass (kg)**	**Height (cm)**	**Support (mm)**	**Comment**	**Energy (J)**
2	C	60	2,582	50	0	Broken	12,66
2	C	60	2,532	50	0	Not Broken	12,42

Further studies made with the support condition. In contact condition, while gap between the support and the plate is 0mm. It is observed that total mass needed, increases to 2582 grams while without support 1200grams was sufficient. After testing with 0mm gap, tests done with 2mm, 4mm and 6mm clearances, no dramatic change observed compared to 0mm condition. In vehicle configuration minimum 3mm is allowed due to assembly constraints. Result of this analysis shows positive impact usage of support in case sharp impactor.

Table 4.7: Test 1.6 - 60° 2mm, 4mm, 6mm- support, Type C.

Thickness (mm)	**Ball Type**	**Angle (°)**	**Mass (kg)**	**Height (cm)**	**Support (mm)**	**Comment**	**Energy (J)**
2	C	60	2,532	50	2	Broken	12,42
2	C	60	2,482	50	2	Not broken (NB)	12,17
2	C	60	2,482	50	4	Broken	12,17
2	C	60	2,432	50	4	NB	11,93
2	C	60	2,432	50	6	Broken	11,93
2	C	60	2,382	50	6	NB	11,68

In Test N°2 repetition done with impactor type C2. Target is to verify conicity impact to absorbed energy and comparison with type C. In figures 4-9, 4-10, 4-11, 4-12, 4-13, 4-14, 4-15, 4-16 and 4-17 Test2.1 samples are shown.

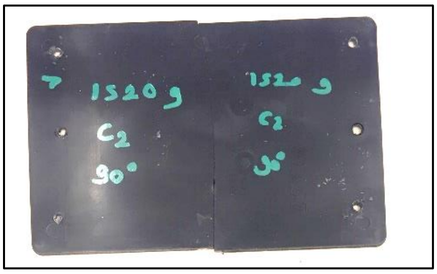

Figure 4.9: Test 2.1 sample. Type C2 1520 gram broken 90°.

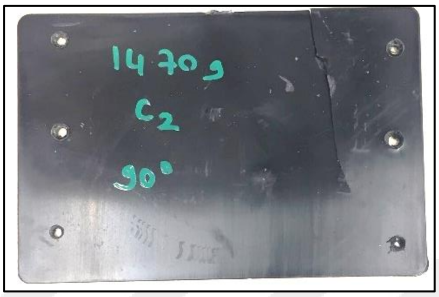

Figure 4.10: Test 2.1 sample. Type C2 1470 gram broken 90°.

Figure 4.11: Test 2.1 sample. Type C2 1370 gram broken 75°.

Figure 4.12: Test 2.1 sample. Type C2 1320 gram broken 60°.

Rear axle cover is under impact loading to due to stones whose source are front wheel during the drive. Depending to the road condition, several stones can touch in same area. To evaluate the repetitive loading condition, in Test N°3 less weight used to drop Type B and TypeB2 impactor compared to the one used in Test N°1.1 with repetition. According to the results, while Type B in 768 grams can break the plate in single shot, 718 grams is able to break the plate in 8 & 9 shots. While Type B2 in 768 grams can break the plate in single shot, 718 grams can break plate in 13 & 15 shots. 7% delta is calculated compared to single shooting. According to results, flat ending tip requires less repetition.

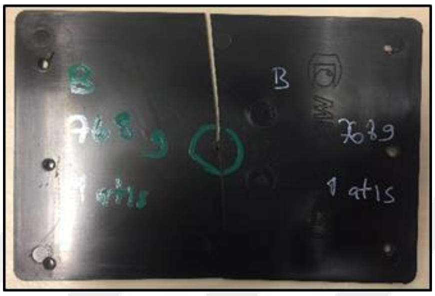

Figure 4.13: Test 3.1 Type B, 90° single shot, 768g.

-

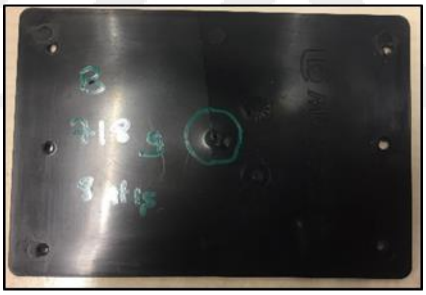

Figure 4.14: Test 3.1 Type B, 90° 8 shot 37 s, 718g.

Figure 4.15: Test 3.1 Type B, 90° 9 shots, 718g.

Figure 4.16: Test 3. Type B2, 90° 1 shots, 768g.

Figure 4.17: Test 3.2 Type B2, 90° 13 shots, 718g.

Figure 4.18: Test 3.2 Type B2, 90° 15 shots, 718g.

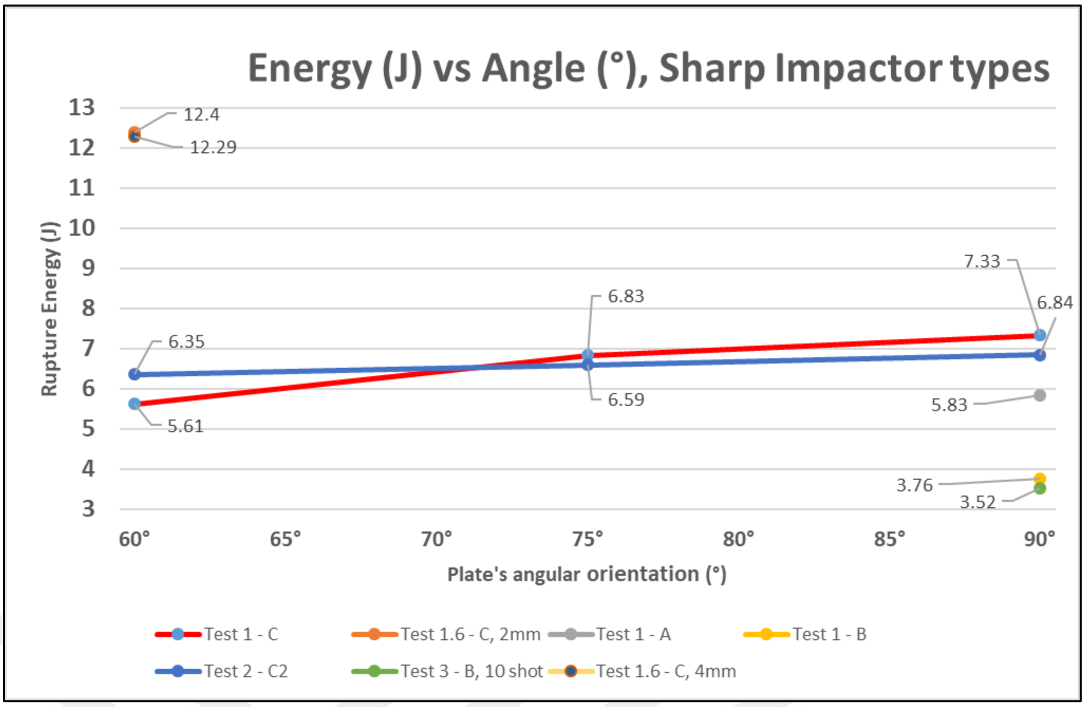

Figure 4.19: Test 1, Test 2, Test 3 Synthesis.

According to Test 1, Test 2, Test 3; it is obvious that angle is proportional to the breakage energy. When the impactor profile changes from blunt to pointed, the target plate's fracture energy decreases. Any increase on the conciality of the impactor results with reduced rupture energy. With repetition, less energy may be sufficient to break the same piece as seen in Figure 4-19.

4.4. Test with Spherical Impactor

Following the same procedure, Test 1 to Test 3, a non-sharp impactor tested with sphere R16 in accordance with OEM specification. With low-speed impact no breakage was detected at 50cm. Using 60°, 75° and 90°, orientation tests repeated from 65cm free fall. Different to the sharp impactors, with sphere type impactor, breakage occurred in fixation points, not in impact area. Beside this, relation of angle & breakage energy was different; more mass needed in case of reduce angle to break the part. In the figure 8-24 Test-4 Sphere test impactor is seen.

Figure 4.20: Test 4, Sphere test impactor.

Figure 4.21: Plate, Test 4 broken sample 1.

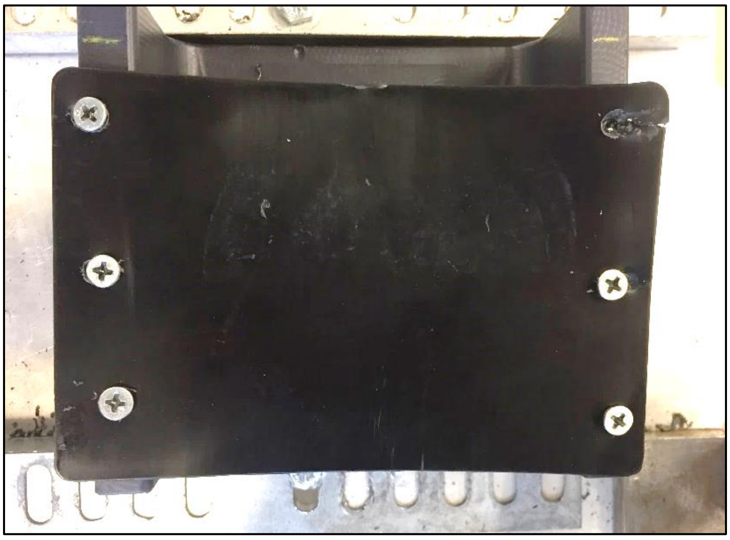

Figure 4.22: Plate, Test 4 broken sample 2.

Table 4.8: Test 4, 65cm results.

Thickness (mm)	Ball Type	Angle (°)	Mass (kg)	Height (cm)	Support (mm)	Comment	Energy (J)
2	D	90	3500-4000	65	50	Broken	-
2	C	75	4500-5000	65	50	Broken	-
2	C	60	5000-5500	65	50	Broken	-

There is an inverse relation between angle and rupture energy with sphere type, while is it proportional in sharp impactor. There is a conflict according to sharpness. Either it is possible to run a multi-objective optimization or assess separately.

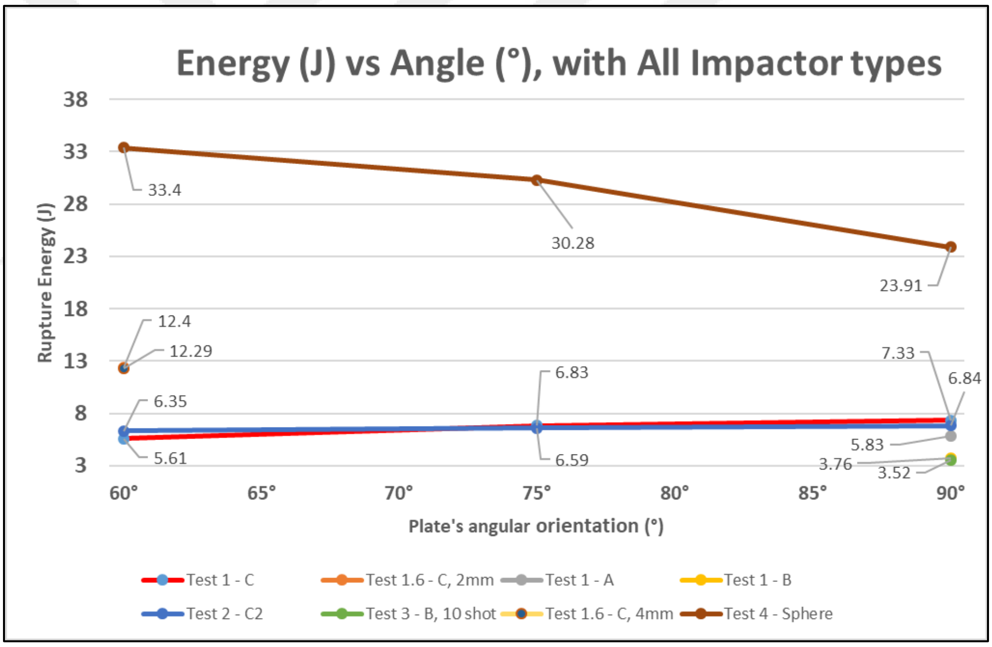

Figure 4.23: Test 1,2,3,4 synthesis.

The type of breakage is different to the one that occurs on actual product. Therefore, it is thought that difference is due to low-speed impact. 2 options reviewed to analyse sphere type impactor case:

Option 1: Physical testing with a horizontal test bench, controlling the speed and using sphere impactor in the diameter and mass defined in OEM specification.

Option 2: Making numerical calculations to evaluate shape difference impact of absorbed energy.

For option 1, a conceptual study done. A spring mechanism is supposed to release the impactor. Plate orientation is adjustable, and speed is read with sensors.

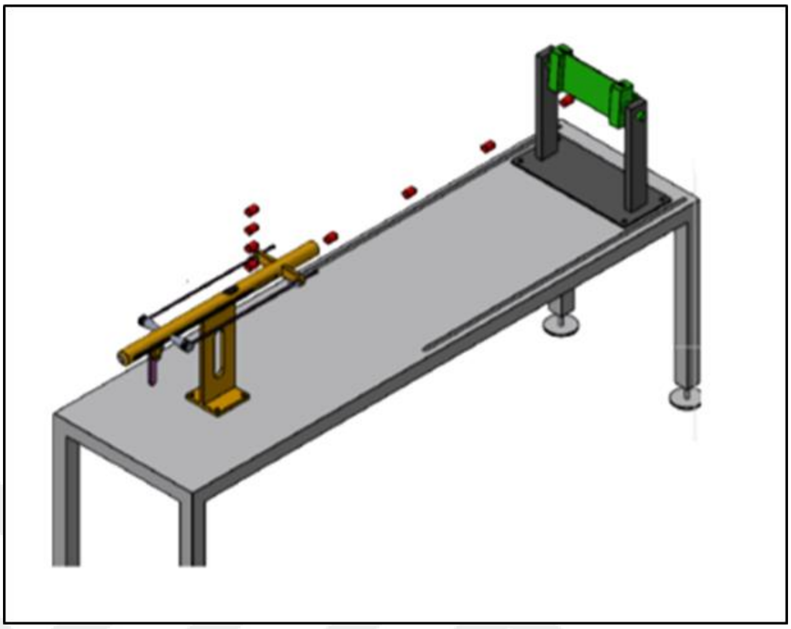

Figure 4.24: Impactor test bench conception.

In option 2, the main difficulty is lack of reliable fracture model for plastics. However, we have elasticity information from tensile tests and while maximum strain is below rupture limit, cracking is not concerned. So, it is possible to make a comparative study to analyse behaviour of absorbed energy due to partially elastic collision, but results will be comparable between each other which are created in same conditions and not the physical tests N1, N2 and N3.

Within the scope of this study, numerical analysis with the finite element method (option 2) is selected.

4.5. Numerical Analyses

Strain rate dependency of PP under impact loading was discussed in section 1.1. In quasi-static region, stress response of PP is sensitive to strain rate however slope of stress-strain curve in elastic region is similar under for different strain rates [20]. Moreover, in intermediate and high velocity impact loadings, change of elasticity modulus is negligible.

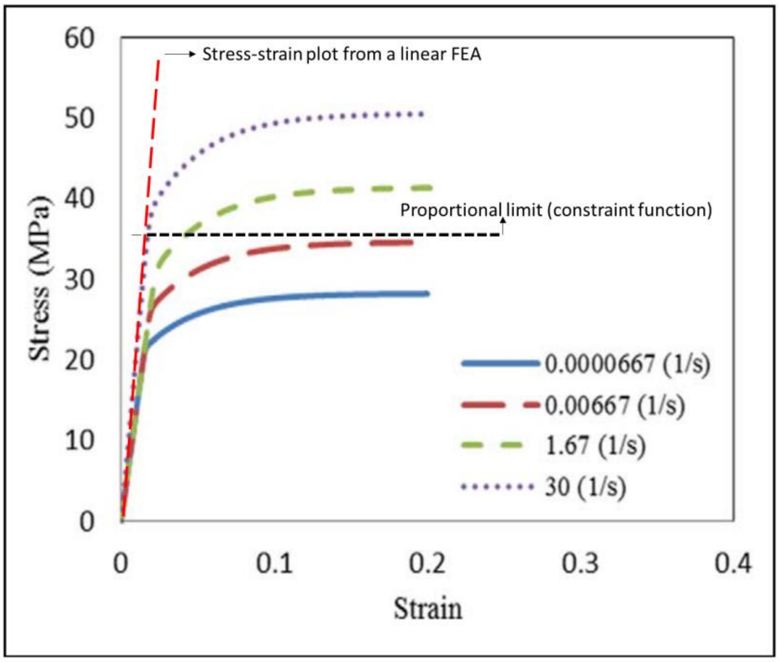

Figure 4.25: Strain rate independency of Young Modulus and optimization approach (reproduced from [25])

To reduce calculation cost, numerous analysis methods have been developed to estimate the local stress–strain responses based on the stress output from a linear, elastic FEA. The stress calculated from a linear, elastic FE analysis is often named pseudo stress or fictitious stress to differentiate the true stress as plasticity occurs [56]. Due to strain rate independency of Young modulus, pseudo-stress calculations are performed in the scope of the thesis. If the nonlinear curve were taken into account, the strain here defined as a constraint function in the optimization problem which increases the computational costs. In pseudo-stress approach, if stress is constrained to the proportional limit conservatively, failure of the product is avoided.

4.6. Numerical Analyses on Parametric Plate Model

A plate 2D model has been created, representatively to the physical test. and 2D mesh created via Ansys Workbench software with 2mm element size. Raw material of for impactor is given as;

Table 4.9: Impactor, properties

$E(MPa)$	$\rho(\frac{kg}{m^3})$	υ	Behaviour
210 000	7850	0.3	Rigid

Table 4.10: Target plate, properties

$E(MPa)$	$\rho(\frac{kg}{m^3})$	υ	$\sigma_y(MPa)$	$\varepsilon_y(\%)$	Behaviour
938	1000	0.4	19.54	6.6	Flexible*

*Non-Linearity is suppressed. Target plate is 100mmx150mm.

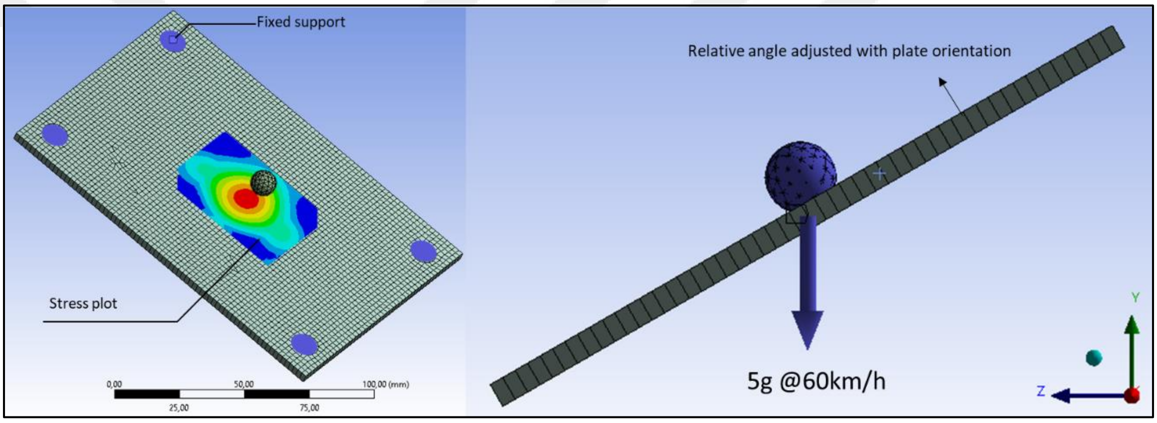

Figure 4.26 : Finite element model of plate

Fixed supports represent bolted joints similar to the plate drop testing. Weight of the ball is 5g and flexibility of the ball is supressed. 20 different analyses are performed. Thickness range is from 1.5mm to 3.5mm which are limit boundaries for injection feasibility and places in table with 0.5mm increments. 4 different angle values are defined with 15° increments. Maximum stress is read from the plate. Final velocity of the ball is calculated. In each analysis, ball orientation is constant. This condition is representing the vehicle condition; a cad simulation made with Catia V5 to understand angular orientation of the gravel and rear axle cover. It has been understood that a stone thrown from the front wheel and coming to the rear of the vehicle can scan an area of 1 degree on the rear axle. This is negligible. Thus, it is assumed that, gravel direction is constant and relative angle is set by product orientation.

Table 4.11: Results of numerical analyses, plate

Thickness(mm)	Angle (°)	Stress (MPa)	Final Velocity (mm/s)
1.5	90	43.435	7935.4
2	90	28.173	5764
2.5	90	23.199	7818.4
3	90	14.784	7295.8
3.5	90	12.559	6568.2
1.5	75	40.624	8339.2
2	75	27.894	7581.6
2.5	75	23.512	8496.2
3	75	14.881	8487.9
3.5	75	13.659	8324.3
1.5	60	40.516	11503
2	60	25.99	11691
2.5	60	21.285	11616
3	60	15.089	11368
3.5	60	13.196	11414
1.5	45	30.51	12993
2	45	20.833	13942
2.5	45	19.309	14475
3	45	13.407	13379
3.5	45	9.84	13775

4.7. Numerical Analyses of Partial Rear Axle Cover Model

A partial rear axle cover 3D mathematical model has been created and 2D mesh created via Hypermesh software with 2.5mm element size. Raw material for impactor is given as:

Non-Linear behaviour is selected. Tensile curve is as given below.

Table 4.12: Impactor, properties

$E(MPa)$	$\rho(\frac{kg}{m^3})$	ν	Behaviour
210 000	7850	0.3	Rigid

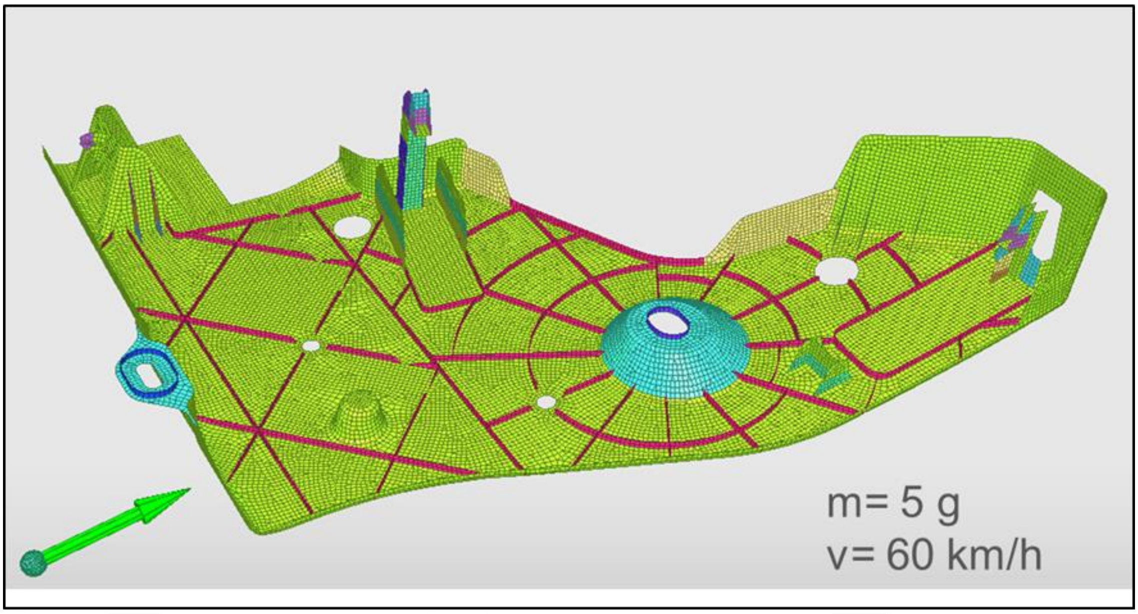

Figure 4.27: Finite Element Model

Table 4.13: Target plate, properties

$E(MPa)$	$\rho(\frac{kg}{m^3})$	ν	$\sigma_y(MPa)$	$\varepsilon_y(\%)$	Behaviour
938	1000	0.4	19.54	6.6	Flexible*

Tester	: Zwick /Z020	Test machine/Load cell	: Load cell 20 kN
Specimen body	: Flat specimen	Extensometer	: 70 mm
Material	: EMP CP-M 8081	Specimen holders	: ALMEN AŞ
Manufacture/Batch	:	Speed E-Modulus	: 50 mm/min
Pre-treatment	:	Test speed	: 300 mm/min
Test requirements	:		

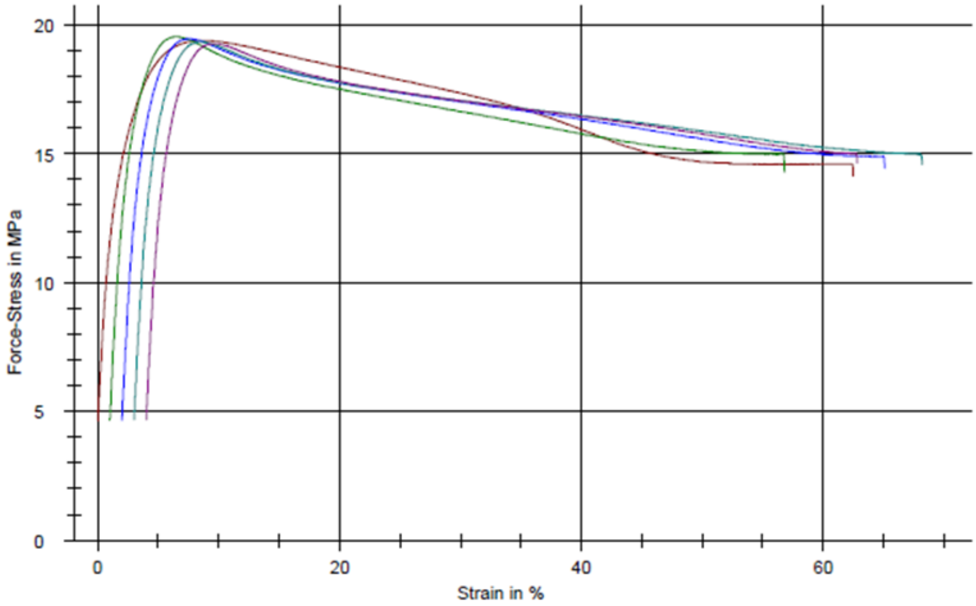

n = 5	Et MPa	σ x N/mm²	σM MPa	εM %	σB MPa	εB %	εtM %	εtB %	L0 mm
x̄	941,54	12,29	19,41	6,58	14,42	61,60	8,15	59,23	70,37
s	18,84	0,64	0,10	1,46	0,20	3,74	1,67	1,72	0,02
ν	2,00	5,19	0,53	22,24	1,41	6,07	20,52	2,90	0,02

Figure 4.28: Stress-Strain curve with 300mm/min.

Result of tensile test at 1mm/min traction speed is as given below, for simulating dynamic case in this study 300mm/min data used.

n = 5	Et MPa	σ x N/mm²	σM MPa	εM %	σB MPa	εB %	εtM %	εtB %	L0 mm
x̄	839,00	12,81	17,77	7,48	13,92	83,92	9,08	76,60	70,36
s	17,95	1,07	0,31	1,18	1,06	4,45	1,27	6,62	0,02
ν	2,14	8,37	1,76	15,73	7,60	5,30	13,95	8,64	0,03

Figure 4.29: Strain Stress curve with 1mm/min.

As seen in Figure 8.27, according to the results, ultimate stress (19.5MPa) is not exceeded (16.2MPa) but yield strain (6.6 %) is exceeded (9.2MPa). So, part is in plastic region with permanent deformation of 2.6% elongation without any breakage risk. In this configuration 0.59J of energy is absorbed while initial kinetic energy was 0.69J.

Energy absorption by part is analysed in Radioss as shown

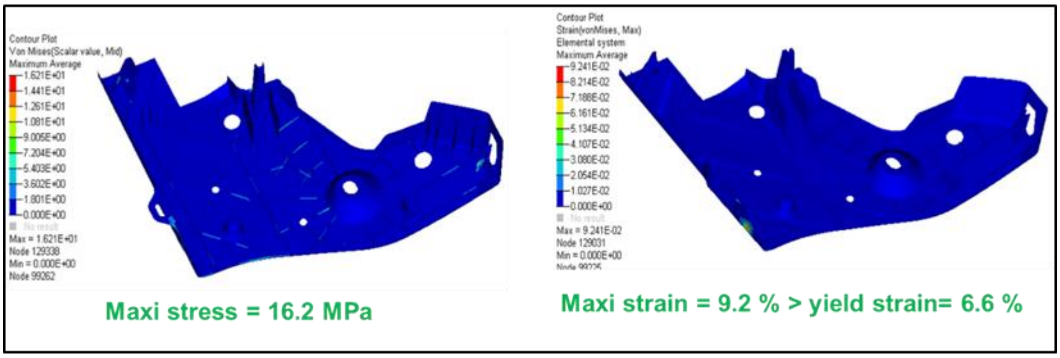

Figure 4.30: Analysis 1 Maximum Stress, Strain results.

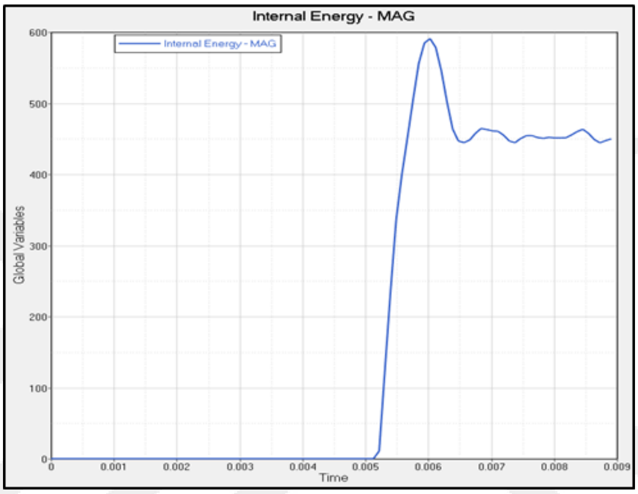

Figure 4.31: Absorbed Energy (by product) 0.59J.

4.8. Numerical Analyses on Parametric Representative Model

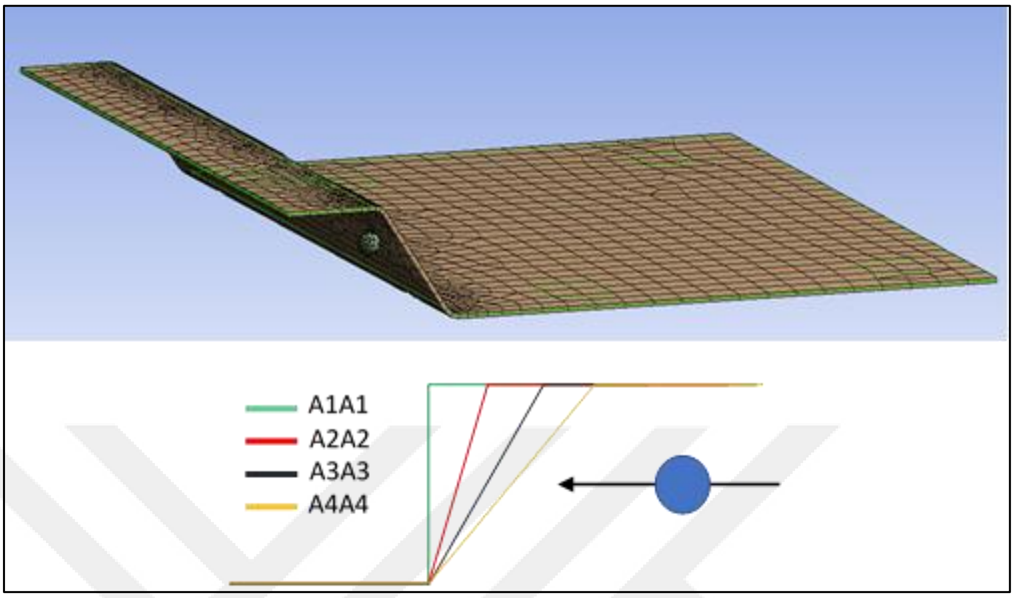

Figure 4.32: Parametric Models for Explicit Analysis

A new, parametric, 2D geometry is modelled, which is representative of the partial rear axle cover. This new model has similar dimensions to the partial rear axle cover model seen in Figure 4.27. Initially 4 base profiles; A1A1, A2A2, A3A3 and A4A4 (figure 4.32) are created to be used in analysis.

Mathematical models created with base profiles are shell-structured geometries. Thickness variations were created with analysis software. Combinations with all thickness and angle variations are shown in Table 4.11. The stress on the target plate and the final velocity of the striker were calculated using the Explicit Dynamics module of Ansys software. Below parameters considered in the analysis;

Table 4.14: Impactor, properties

$E(MPa)$	$\rho(\frac{kg}{m^3})$	υ	v_0(mm/s)	m(g)	Behaviour
210 000	7850	0.3	16666	5	Rigid

Table 4.15: Target plate, properties

$E(Pa)$	$\rho(\frac{kg}{m^3})$	υ	$\sigma_y(MPa)$	$\varepsilon_y(\%)$	Behaviour
9.15E+08	902	0.443	19.54	6.6	Flexible*

Hence impactor is defined as rigid material, elasticity of ball is ignored.

Total analyses time is given as 0.007s and 20 steps used in calculations. Mesh convergence made for first model A1A1, it is noted that default mesh size is ok for convergence. Contact points are reflected from Radioss model and in each model size of contacts and positions are kept.

Table 4.16: Mesh Details for Analysis

Impactor Nodes Quantity	71
Impactor Number of elements	213
Part Nodes Quantity	2078
Part Number of elements	2037
Element Size Part (average)	6,55

Table 4.17: Results of the numerical analyses

Type	Thickness (mm)	Angle (°)	Stress (MPa)	Final Velocity (mm/s)
A1A1-1,5	1.5	90	27.73	7607
A1A1	2	90	26.50	8068.3
A1A1-2,5	2.5	90	21.27	8021.6
A1A1-3	3	90	17.42	7926.8
A2A2-1,5	1.5	75	29.74	8541.6
A2A2	2	75	23.90	9134.8
A2A2-2,5	2.5	75	19.55	9170.4
A2A2-3	3	75	18.57	10054
A3A3-1,5	1.5	60	23.56	10035
A3A3	2	60	16.48	10052
A3A3-2,5	2.5	60	13.89	10566
A3A3-3	3	60	12.54	10186
A4A4-1,5	1.5	45	15.27	12689
A4A4	2	45	13.22	12920
A4A4-2,5	2.5	45	10.60	13304
A4A4-3	3	45	7.25	13448

5. CURVE FITTING and OPTIMIZATION

The response surface was created with the Von Misses stress values (Table 4.2) obtained as a result of the analyses made with the plate model (Section 4.6, the model that is the equivalent of the plate used in the physical experiment). Response surface was created with the thickness and angle parameters shown in (5.1).

The 3rd order polynomial (5.1) response surface f_1 is (Figure 5.1) created with Matlab with a fitting quality of $R = 0.981$, where thickness is t, angle is a and $\sigma$is Von-Misses Stress.

$$f_1(t, a) = \sigma \tag{5.1}$$

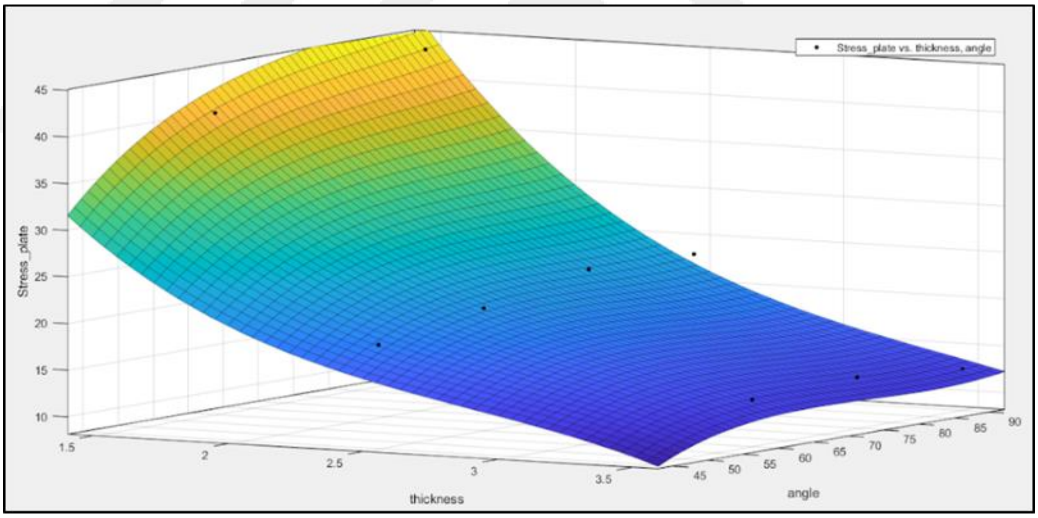

Figure 5.1: Stress response surface to thickness and angle, plate 2D model

f_2 is mass which is function of dimensions and thickness,

$$f_2 = \frac{t * 100 * 150}{1000} \tag{5.2}$$

f_3 is rupture energy which is obtained from physical impact testing. Curve fitting study made and the formula is given below (5.3).

$$f_3(t,a) = -7.769 + 0.6653 * t + 0.2879 * a - 0.121 * t^2 + 0.01193 * t * a - 0.00171 * a^2 \quad (5.3)$$

The weight factors and normalization factors are implemented to the equation 3.12 and equation 5.4 is obtained.

The thickness parameter is included in all three sub-functions in the composite function. In two of these sub-functions, the increase in thickness resulted in minimizing the stress and maximizing the fracture energy. Therefore, it participates positively twice in the composite function. Due to this situation arising from the structure of the composite function, the weight factor of the mass function is adjusted as the sum of the other two sub-functions. Weight factors are selected as;

$w_1 = 0.25, w_2 = 0.5, w_3 = 0.25$

Normalization factors values of objective functions are;
$sf_1 = 22.62, sf_2 = 37.5, sf_3 = 6.25$

$$f(t,a) = \frac{f_1}{45.24} + \frac{f_2}{75} - \frac{f_3}{26} \rightarrow min \quad (5.4)$$

f_3, rupture energy, is aimed to be maximized, therefore has a minus sign. (5.4). Constraint function (5.5) and (5.6) are manufacturing and design constraints. (5.7) is constraining proportional limit from numerical analysis.

$$1.5 \leq t \leq 3.5 \quad (5.5)$$

$$45 \leq a \leq 90 \quad (5.6)$$

$$f_1 \leq 25 \quad (5.7)$$

The composite $f(t, a)$ objective function (5.4), which is created by combining the experimental and analysis data is used to create the response surface. Fitting quality of the response surface is 0.9989.

This function solved in Matlab using a with a local optimization method and $t = 2.2mm$, $a = 90°$ is found as best design parameters to have minimum stress and lightweight product.

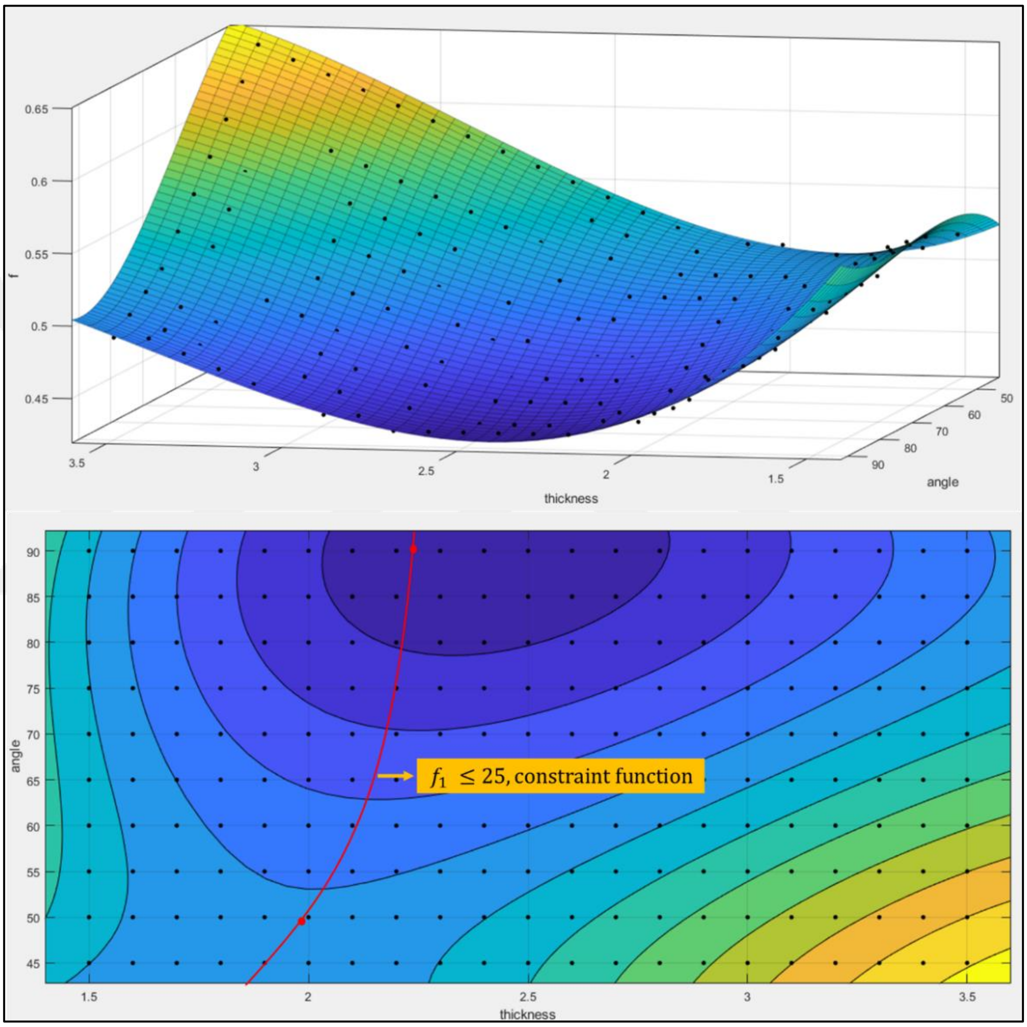

Figure 5.2: Optimization for plate analysis, mass and rupture energy

Curve fitting made from data obtained in section 4.8.

It is noted that stress results are more suitable to make curve fitting as seen in Figure 5.3.

2D plate model and rear axle cover model have different boundary conditions. Plate 2D model has equal boundary condition with the target plate which is used in experimental studies. Response surface of rear axle cover representative model is also created using same thickness and angle variables.

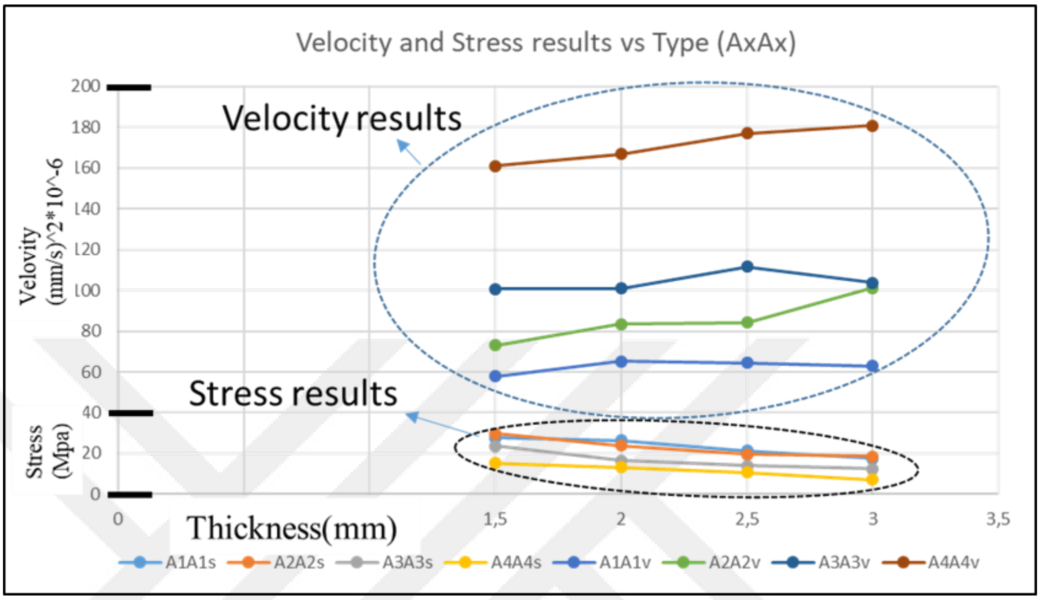

Figure 5.3: Stress and velocity vs Geometry Tpye AxAx

A response surface analysis done in Matlab software to create results for any design parameter as shown in Figure 5.4. Quality error for this curve fitting is R=0.95.

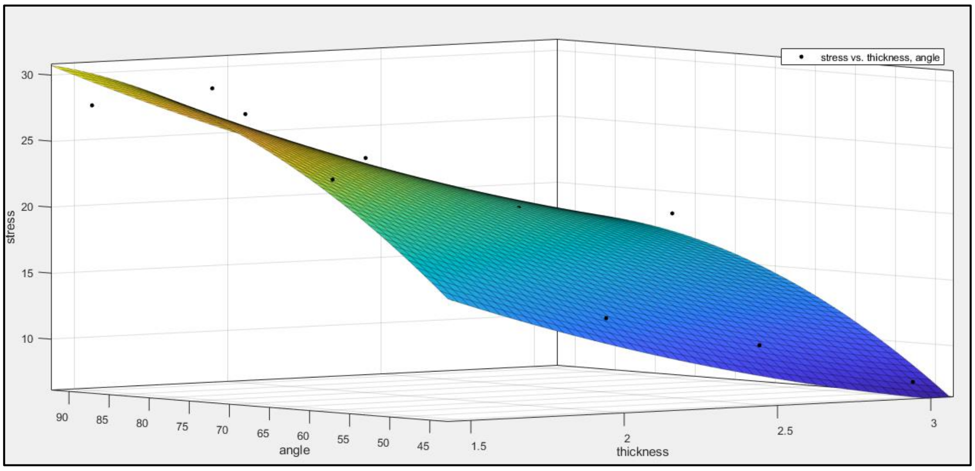

Figure 5.4: Response surface of stress to angle & stress

Comparison of the stress response surfaces in different boundary conditions is given in Figure 5.5. These stress results are f_1, which is input in composite function given in equation 3.12.

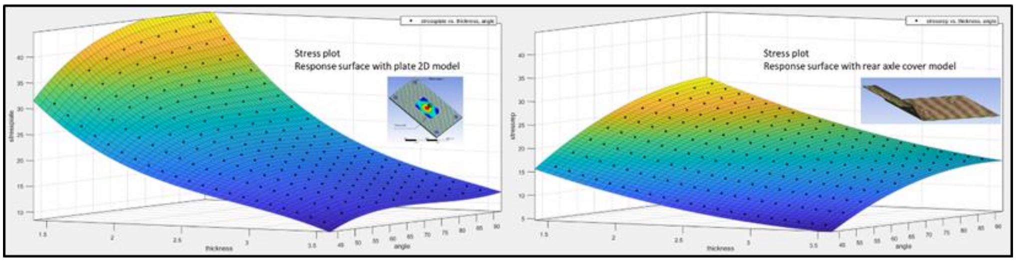

Figure 5.5: Response surface comparison of plate 2D model and rear axle cover model in different boundary conditions

Effect of different boundary condition to optimum design parameter search is investigated. Comparison is given in Figure 5.6. In this comparison each functions have same weight factors, normalization factors of stresses are different. It is found that the response surface largely depends on the boundary conditions.

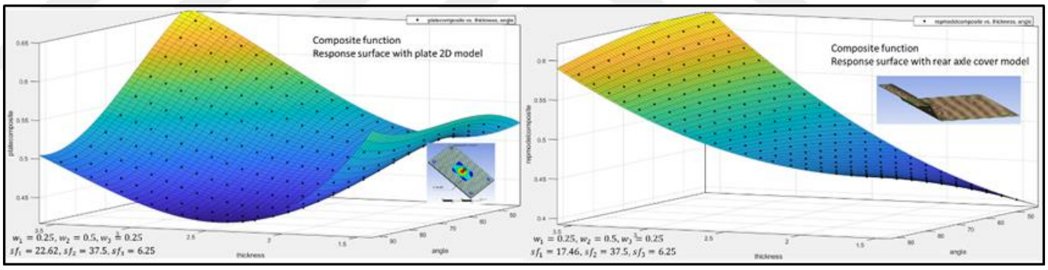

Figure 5.6: Response surface comparison of composite function, stress model obtained from plate analysis vs stress model obtained from representative rear axle model, same weight factors.

Effect of the weight factors to the optimum design parameter search is investigated. Comparison is given in Figure 5.7. Response surface is highly depended on weight factors.

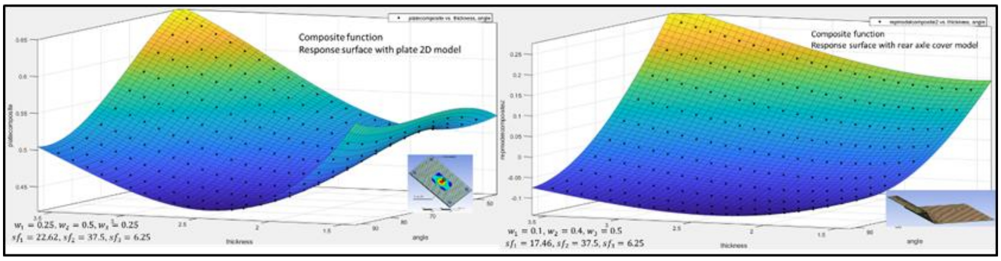

Figure 5.7: Response surface comparison of composite function, stress model obtained from plate analysis vs stress model obtained from representative rear axle model, different weight factors.

As seen in Figure 5.5, Figure 5.6 and Figure 5.7 optimum angle parameter is always 45° or 90°. With different weight factors, either f_1 (stress function) or f_3 (energy function) is dominating the composite function. Weight sum methodology, is not capable to select a balanced angle value between given upper and lower limits, thus composite function is highly dependent to weight factors. With help of this information and above comparisons, it is learned that the boundary conditions of the target plates to be used in experimental and numerical studies should be the same. It is predicted that the difference in the response surfaces obtained from the composite functions and their dependence on the weight factors are due to the fact that the normalization factors cannot be determined comprehensively to be used for solving problems in different boundary conditions. The derivative of the mass functions in the composite function are the same for the two problems and is independent in the boundary conditions. However, stress behaviour under intermediate velocity impact loading varies and this causes also differences in results.

6. CONCLUSION and RECOMMENDATIONS

In this thesis, the behaviour of a plastic part under impact load, exposed to different types of impactors, was investigated and optimization possibilities were investigated. As a result of experimental and numerical analysis studies with target plates with different geometries, the effect of thickness and angle variables was measured. Important conclusions are recorded. Thickness increase has positive impact on gravel resistance both for sharp and sphere type impactors. Limited deflection with stoppers is increasing the energy to break the part both for sharp and sphere impactors. While perpendicularity is inversely proportional to breakage energy for sharp impactor, in case of sphere impactor absorbed energy is proportional to perpendicularity. Design and manufacturing limits are clear for this engineering problem, it is noted that, constrained optimization techniques are suitable for investigating optimum design parameters.

Within the scope of the thesis study, one of the fracture types of the plastic part was focused. Abstractions and simplifications were made in order to carry out optimization work. In this context, more comprehensive studies are needed in which all phenomena are taken into account.

- In scope to the thesis work, numerical and experimental studies performed in different velocity and different impactor geometry. In order to compare the same loading types experimentally and numerically, the current conditions are not sufficient and a ballistic test setup should be established.
- Only one raw material was used in this study. In the proposed physical impact testing with a specific bench, different raw materials should be tested to optimize material.
- Plate 2D model and partial rear axle cover model analysed with uniform thickness assumption. Topology optimization should be done to limit material increase.
- In the selected scenario impactor hits on a flat surface. Effect of curved surfaces in concave and convex form should be investigated.
- In experimental and numerical approach, mainly single impactor was analysed. In real condition. Multiple impactor case should be studied experimentally and

numerically to understand the effect of repetition to residual stresses and permanent deformations.

- Weight-sum methodology is not capable to propose optimum angle parameter and creating results in extremities. Therefore; energy function could be considered as constraint instead of being used in composite function or other multi-objective optimization methodologies should be studied.

REFERENCES

[1] Akshat P., Arun P., Rajesh P., (2017). "An overview of Polymeric Materials for Automotive Applications." Materials Today: Proceedings, 4(2), 3807–3815.

[2] Joost W., (2012). "Reducing Vehicle Weight and Improving U.S. Energy Efficiency Using Integrated Computational Materials Engineering." JOM: the journal of the Minerals, Metals & Materials Society, 64(9), 1032–1038.

[3] Emilsson E., Dahllöf L., Ljunggren M., (2019). "Plastics in passenger cars A comparison over types and time." Report number C 454, Affiliation: IVL Swedish Environmental Research Institute

[4] Maddah H., (2016). "Polypropylene as a Promising Plastic: A Review." American Journal of Polymer Science 2016, 6(1): 1-11.

[5] Gervet B., Nordell, B., (2022). "THE USE OF CRUDE OIL IN PLASTIC MAKING CONTRIBUTES TO GLOBAL WARMING." International Journal of Global Warming. Vol. 1, Nos. 1/2/3 378-391.

[6] Mihai M., Stoeffler K., (2017). "Eco-solutions for automotive interior applications by way of thermoplastic biocomposites: cost, weight and green advancements." International Journal of Automotive Composites. 3(2-4).

[7] Wang W., Zeng Y., (2020). "Introductory Chapter: Polypropylene - Synthesis and Functionalization. Polypropylene - Polymerization and Characterization of Mechanical and Thermal Properties." IntechOpen, London (1-8).

[8] Jansz J., (1999). "Polypropylene in automotive applications." Polymer Science and Technology Series. Polypropylene, 643–651.

[9] Hopewell J., Dvorak R., Kosior E., (2009). "Plastics Recycling: Challenges and Opportunities." Philosophical transactions of the Royal Society of London. Series B, Biological sciences. 364. 2115-26. 1

[10] Garbelli M., (2016). "Managing Sustainability to Be First: The Toyota Case." In book: Business Challenges in the Changing Economic Landscape - Vol. 2. 41-54.

[11] Ladhari A., Kucukpinar E., Stoll H., Sängerlaub S., (2021). "Recycling Comparison of Properties with Relevance for the Automotive Sector in Mechanically Recycled and Virgin Polypropylene." MPDI Recycling Journal. 6, 76.

[12] Kurtaran H., Buyuk M., Eskandarian A., (2003). "Ballistic impact simulation of GT model vehicle door using finite element method." Theoretical and Applied Fracture Mechanics. 40. 113-121.

[13] Ali A., Sanuddin A., Yee B., Afshar R., (2012). "Simulation of an impact test for PC-PET plastic." Recent Trends in Fracture Mechanics. 127-139.

[14] Vaidya U., (2011). "Impact Response of Laminated and Sandwich Composites." CISM International Centre for Mechanical Sciences, Courses and Lectures. 526.

[15] Cantwell J., Morton J., (1991). "The impact resistance of composite materials a review." Composites, 22(5), 347–362.

[16] Liu D., Malvern E., (1987). "Matrix Cracking in Impacted Glass/Epoxy Plates." Journal of Composite Materials, 21(7), 594–609.

[17] Kurtaran H., Buyuk M., Eskandarian A., (2003). "Design automation of a laminated armor for best impact performance using approximate optimization method." International Journal of Impact Engineering - INT J IMPACT ENG. 29. 397-406.

[18] Mohd O., Hazizan A., Zainal A., (2011). "Measurement and prediction of compressive properties of polymers at high strain rate loading." Materials and Design, 32(8-9), 4207–4215.

[19] Gebremeskel A., Asija N., Chouhan H., Bhatnagar N., (2018). "Polypropylene nano-composites at high strain rate impacts: Characterization, failure modes, and modeling." Momona Ethiopian Journal of Science, 10(1), 28–50.

[20] Shokrieh M., Joneidi A., Mosalmani R., (2015). "Characterization and simulation of tensile behavior of graphene/polypropylene nanocomposites using a novel strain-rate-dependent micromechanics model." Journal of Thermoplastic Composite Materials, 28(6), 818–834.

[21] Daiyan H., Andreassen E., Grytten F., Lyngstad O., Luksepp T., Osnes H., (2010). "Low-velocity impact response of injection-moulded polypropylene plates – Part 2: Effects of moulding conditions, striker geometry, clamping, surface texture, weld line and paint. Polymer Testing "- POLYM TEST. 29. 894-901.

[22] Alcock B., Cabrera N., Barkoula M., Peijs T., (2006). "Low velocity impact performance of recyclable all-polypropylene composites." Composites Science and Technology. 66. 1724-1737.

[23] Fernando L., Williams G., (1980). "Plane stress and plane strain fractures in polypropylene." Polymer Engineering and Science, 20(3), 215–220.

[24] Fernando L., (1988). “Fracture toughness of filled polypropylene copolymer systems.” Polymer Engineering and Science, 28(12), 806–814.

[25] Chu Y. Ju., Hyo J. E., Seung Y. Lee., (2018). “Prediction of Damage to the Vehicle Underbody Due to Stone Chipping.” Applied Sciences (Switzerland) 8(10):1–12.

[26] 37/03 002 / B ‘RESISTANCE AU GRAVILLONNAGE SUR PI STE-Renault Norme

[27] Web1, (2021), https://www.slideshare.net/NorbertGruen/fisitaf2010c098norbertgruenpresentationstatic-47880545 (Access date: 12/12/2021)

[28] Vadori R., (2010). “On the Simulation of the Effects of the ‘Stone Chipping’ on the Car Underbody – An Application of Montecarlo Methods.” SAE Technical Paper Series [SAE International SAE 2010 World Congress & Exhibition], 1(), –.

[29] Hartl A. M., Jerabek M., Lang R. W., (2015.) “Anisotropy and Compression/Tension Asymmetry of PP Containing Soft and Hard Particles and Short Glass Fibers.” Express Polymer Letters 9(7):658–70.

[30] Jung W. Y., Weon J. I., (2013), “Impact Performance and Toughening Mechanisms of Toughness-Tailored Polypropylene Impact Copolymers.” Journal of Materials Science 48(3):1275–82.

[31] Lehmann B., Friedrich K., Wu C. L., Zhang M. Q., Rong M. Z., (2003). “Improvement of notch toughness of low nano-SiO2filled polypropylene composites.” Journal Of Materials Science Letters, 22(14), 1027–1030.

[32] Yong L., Chen H., Chan C. M., Wu J., (2008). “High Impact Toughness Polypropylene/CaCO3 Nanocomposites and the Toughening Mechanism.” Macromolecules 41(23):9204–13.

[33] Faramarz A. G., Ismail G., Saman M., Mohsen A., Alireza A., (2016). “Optimization of mechanical properties of polypropylene/talc/graphene composites using response surface methodology.” Polymer Testing, 53(), 283–292.

[34] Sittichai S., (2001). “Advanced Mechanics of Materials.” 1st Edition, Suranaree University of Technology Publication.

[35] Keith N., Richard B., Budynas, (2015). “Shigley's Mechanical Engineering Design”, 10th Edition, McGraw-Hill.

[36] Patel N. M., Byung S. K., Renaud J., Tovar A., (2009). “Crashworthiness Design Using Topology Optimization.” Journal of Mechanical Design, Transactions of the ASME 131(6):0610131–312.

[37] Web2, (2021), https://en.wikipedia.org/wiki/Toughness (Access date: 12/12/2021)

[38] Web3, (2017), https://polymerinnovationblog.com/characterization-thermosets-part-21-tensile-testing-polymers-molecular-interpretation (Access date: 12/12/2021)

[39] Zweben C., Smith W. S., Wardle M. W., (1979). "Test methods for fiber tensile strength, composite flexural modulus, and properties of fabric-reinforced laminates" Composite Materials: Testing and Design (Fifth Conference), ASTM International 228-228–235

[40] Tong C., (2019) "Fundamentals of Materials and Their Characterization Methodologies for Energy Systems. In: Introduction to Materials for Advanced Energy Systems." Springer, Cham, 87-170.

[41] Wilson R., Pfohl W., (2000). "Study of cross-linking reactions of melamine/formaldehyde resin with hydroxyl functional polyester by generalized 2-D infrared spectroscopy1. Vibrational Spectroscopy." 23. 13–22.

[42] Zinzow W. A., Hazen T., (1935) "Electrical Properties of Certain Bakelite Materials" Industrial & Engineering Chemistry 1935, 27 (8), 899-902

[43] Khalil, H.A., Banerjee, A., Saurabh, C.K., Tye, Y.Y., Suriani, A.B., Mohamed, A., (2018). "Biodegradable films for fruits and vegetables packaging application: preparation and properties." Food Engineering Reviews, 10, 139–153

[44] Novares Training Document (2012): -TRAINING-PP-PA- MATERIAL-CGY-JFC-20191211.pdf

[45] (ANSYS Theory Manual 2006)

[46] Tekkaya A. E., Soyarslan C. (2014) "Finite Element Method. In: The International Academy for Production Engineering," CIRP Encyclopedia of Production Engineering. 508-514.

[47] Arora J. S., (1987) "Introduction to Optimum Design" 7th Edition, McGraw-Hill.

[48] Balaban H., Kurtaran H., (2006) "Beyaz Eşya Sektöründe Uygulanan Düşürme Testlerinin Bilgisayarda Simulasyonu" Yüksek Lisans Tezi, Gebze Yüksek Teknoloji Enstitüsü.

[49] Büyük M., Kurtaran H., (2003) "Çarpışma Yükü Altındaki Yapıların Sonlu Elemanlar Metodu ile Analizi ve Optimum Tasarımı" Yüksek Lisans Tezi, Gebze Yüksek Teknoloji Enstitüsü.

[50] Hallquist J. O., (2006) "LS-DYNA Theory Manual. Livermore Software Technology Corporation (LSTC)." 1st Edition, Livermore.

[51] Trivellato F., Castelli M. R., , (2014) "On the Courant–Friedrichs–Lewy criterion of rotating grids in 2D vertical-axis wind turbine analysis." Renewable Energy, Volume 62.

[52] Belegundu A., Chandrupatla T., (2019). "Optimization Concepts and Applications in Engineering "(3rd ed.). P1 Cambridge: Cambridge University Press.

[53] Yang X., (2014). "Nature-Inspired Optimization Algorithms || Multi-Objective Optimization. ", (), 197–211.

[54] Grodzevich O., Romanko O., (2006) "Normalization and other topics in multi-objective optimization." In: The Fields-MITACS Industrial Problems Workshop. 2161-2166

[55] Kappatou C. D., (2017). "Dynamic Optimization of the Production of Monoclonal Antibodies in Semi-batch Operation." [Computer Aided Chemical Engineering] 27th European Symposium on Computer Aided Process Engineering Volume 40 ||, 2161–2166.

[56] Lee Y. L., (2012). "Metal Fatigue Analysis Handbook || Pseudo Stress Analysis Techniques." , 61–87.

BIOGRAPHY

Uğur Şahinkaya was graduated from Yildiz Technical University Mechanical Engineering Department in 2010. Same year he started master's studies on Gebze Technical University in Mechanical Engineering Department.

From 2010 to 2022, he worked for automotive Tier 1 companies in Engineering departments. Since February 2022, he is working for General Electric Aviation as Advanced Lead Engineer.

APPENDICES

Appendix A: Conference Presentation from Thesis Study

Sahinkaya U., (2021), "Design optimization of a plastic cover under impact loading", 6th International Mediterranean Science and Engineering Congress (IMSEC 2021),, Pages: 1-1, Paper ID:125 25-27 October

Appendix B: Figures and Tables

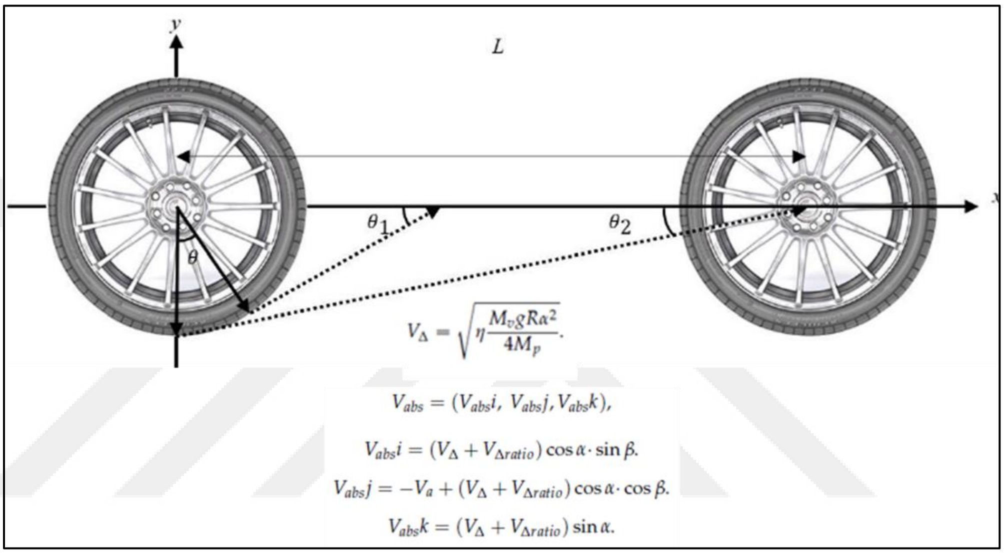

Figure B1.1: Stone speed calculation study.

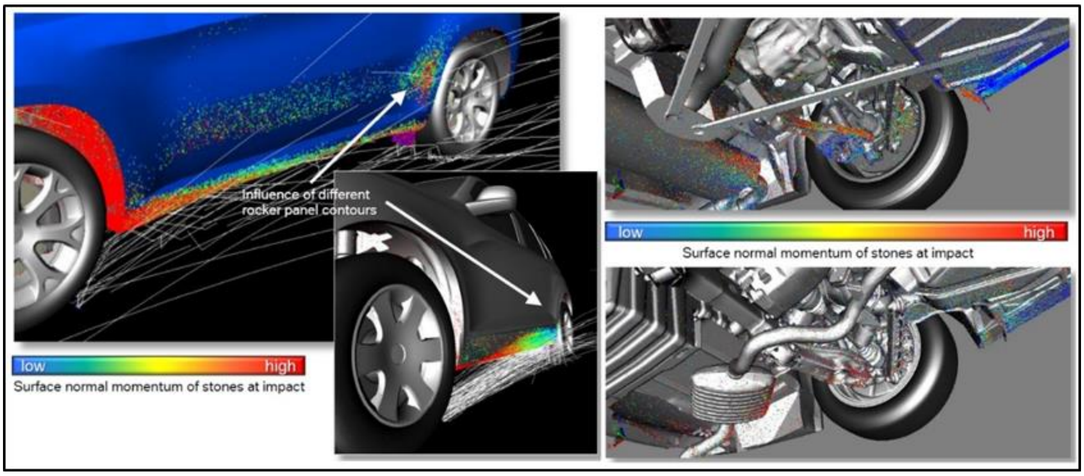

Figure B1.2: Damage probability study example.

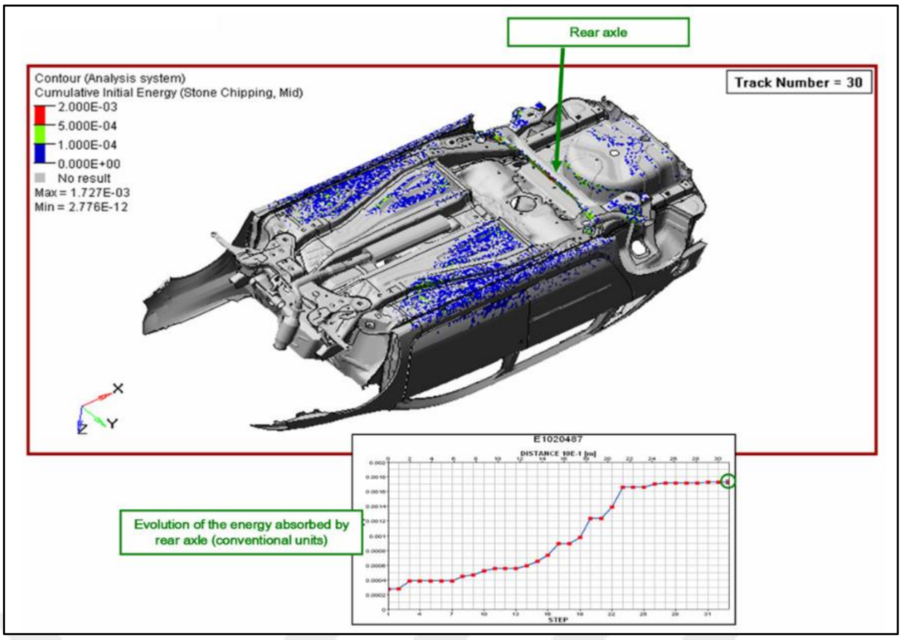

Figure B1.3: Cumulative of absorbed energy and contour plot of the underbody (Vadori, 2010).

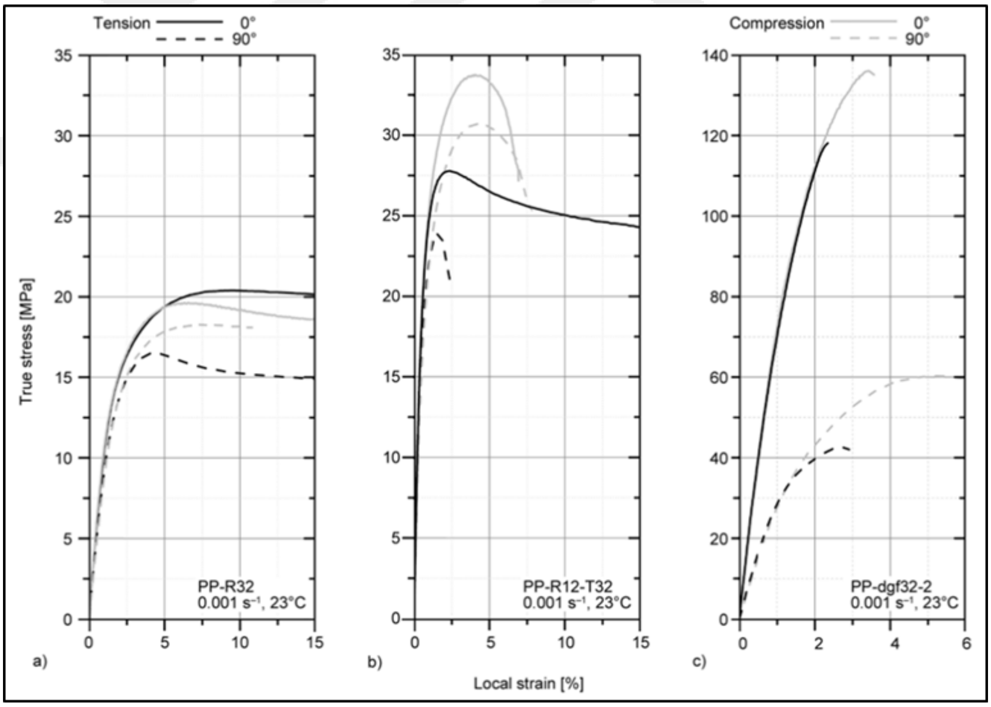

Figure B1.4: Stress- strain trends in compression and tension of PP-R32 (a); PPR12-T10 (b) and PP-sgf32-2 (c).

Composite types: PP filled with		Rubber	Rubber and talc		Short glass fiber	
Material designation and filler characteristics		PP-R32	PP-R27-T10	PP-R12-T32	PP-sgf32-1	PP-sgf32-2
Rubber	content shape	32 w%	27 w%	12 w%		
			elliptic shape			
Talc	content shape		10 w% platelet	32 w% platelet		
Glass fibers	content aspect ratio				32 w% 23	32 w% 32

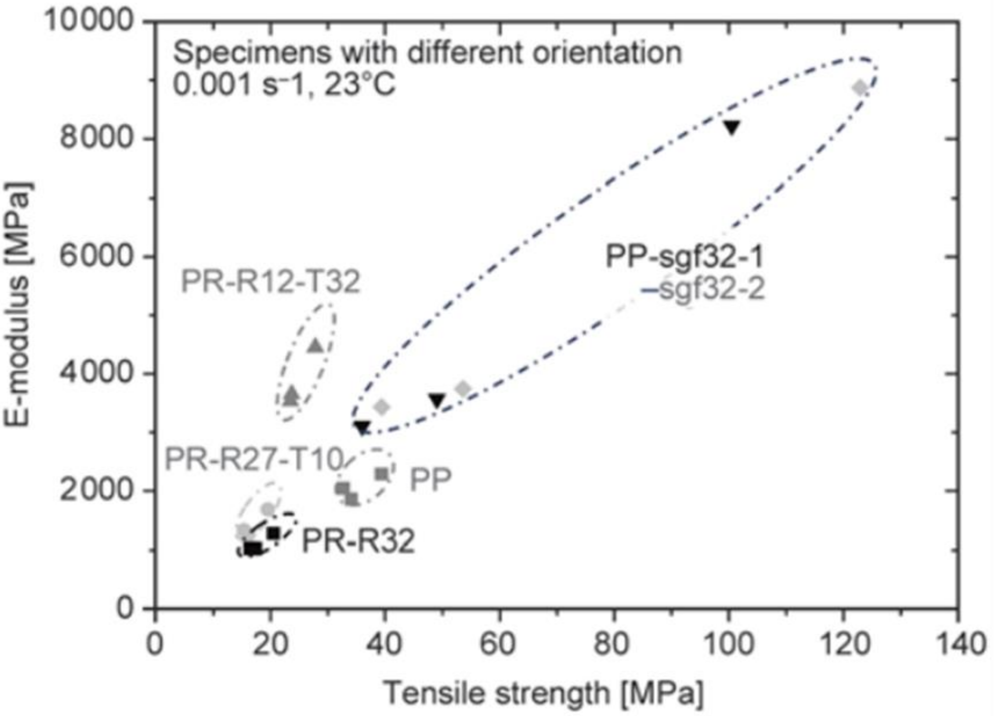

Figure B1.5: Overall illustration of mechanical anisotropy of all materials investigated in terms of tensile modulus versus tensile strength.

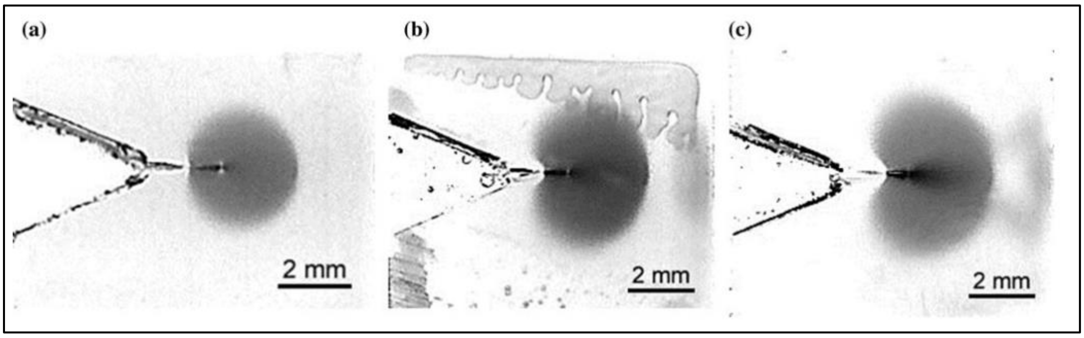

Figure B1.6: Transmitted optical stereo micrographs of DN-4PB Charpy impact-tested damage zone at 0 °C for three ICP blends: a neat ICP, b ICP/ 30.

,

Table B1.1: Impact strength of the ICP and ICP blends sample.

Sample	Impact strength (kJ/m^2)	
	0 °C	−20 °C
Neat ICP	22.6 ± 5	7.0 ± 1.3
ICP/30 %EOC	34.0 ± 9.4	13.7 ± 3.9
ICP/30 %EOC/10 %talc	*N/B*	19.0 ± 5.3

N/B non break (fracture extends less than 90 %)

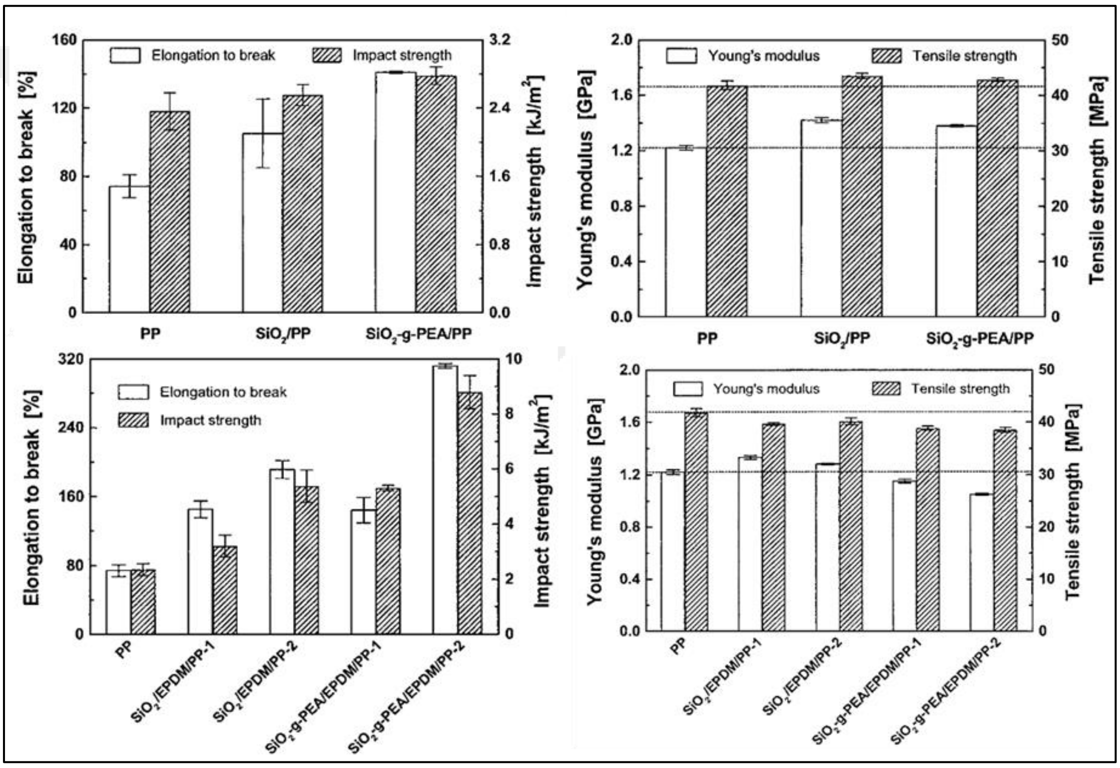

Figure B1.7: Young Modulus, Tensile Strength, Elongation to break and notched Charpy impact strength of PP and its composites filled with nano-SiO2 (content of nano-SiO2 = 0.84 vol%). nano-SiO2 and EPDM (content of nano- SiO2 = 0.84 vol%, content of EPDM for SiO2/EPD.

	Young's modulus (GPa)	yield stress (MPa)	Izod impact strength (J/m)	T_m (°C)	T_c (°C)	crystallinity (wt %)
PP	1.9 ± 0.1	36.3 ± 0.2	38 ± 3	166	115	34.6
annealed PP	2.1 ± 0.1	35.5 ± 0.3	45 ± 5	167	–	40.1
unannealed nanocomposite	2.7 ± 0.1	31.6 ± 0.4	51 ± 5	165	121	33.3
annealed nanocomposite	3.4 ± 0.1	33.5 ± 0.3	168 ± 10	164	–	41.4

Figure B1.8: The mechanical and thermal properties of i-PP and nanocomposites with and without heat treatment.